

THE STRAIN RATE DEPENDENCE UPON GRAIN SIZE  
IN COARSE-GRAIN ZINC

A THESIS

Presented to

The Faculty of the Graduate Division

By

Dennis R. *Richard* Dorman

In Partial Fulfillment

of the Requirements for the Degree

Master of Science

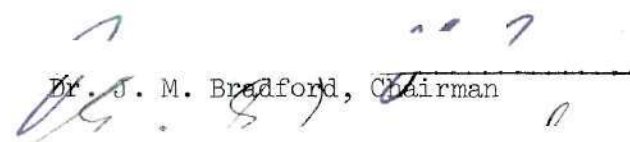
in Mechanical Engineering

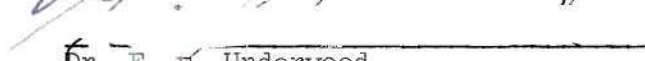
Georgia Institute of Technology

March, 1973

THE STRAIN RATE DEPENDENCE UPON  
GRAIN SIZE IN COARSE-GRAIN ZINC

Approved:

  
Dr. J. M. Bradford, Chairman

  
Dr. E. E. Underwood

  
Dr. R. L. Carlson

Date approved by Chairman: 3-2-73

## ACKNOWLEDGMENTS

I wish to express my appreciation to those who have contributed to the completion of this thesis. The initial work on the subject was done under the guidance of Dr. W. R. Clough (deceased), and completion of the project was accomplished under Dr. J. M. Bradford. I wish to thank them for their advice and encouragement. The reviewing efforts of Drs. E. E. Underwood and R. L. Carlson are greatly appreciated. I also wish to thank the technicians and staff of the School of Mechanical Engineering for their assistance.

A special note of thanks is extended to Mr. S. R. Dunbar of the New Jersey Zinc Company for obtaining the test material used in this investigation.

## TABLE OF CONTENTS

	Page
ACKNOWLEDGMENTS . . . . .	ii
LIST OF TABLES . . . . .	iv
LIST OF ILLUSTRATIONS . . . . .	v
SUMMARY . . . . .	vii
Chapter	
I. INTRODUCTION . . . . .	1
Significance of the Investigation	
Review of Theories of Steady State Creep	
Classification of Specimens	
Herring Theory	
Gilman-Weertman Theory	
Nabarro Theory	
Kosevich-Saralidze-Slezov Theory	
Coble Theory	
Grain Boundary Sliding	
Dislocation Theory	
Statement of the Problem and Attack	
II. EXPERIMENTAL APPARATUS, MATERIAL, AND PROCEDURE . . . . .	21
Review of Constant Stress Creep Machines	
General Description of the Creep Machine	
Testing of the Apparatus	
Specimen Preparation	
Testing Procedure	
III. RESULTS . . . . .	48
Tensile Testing	
Creep Tests on Bamboo Specimens	
Creep Test on Coarse-Grain Polycrystalline Specimens	
Microscopic Investigation of Specimens	

## TABLE OF CONTENTS (Continued)

Chapter	Page
IV. DISCUSSION . . . . .	69
Bamboo Structured Specimens	
Coarse-Grain Polycrystalline Specimens	
V. CONCLUSIONS . . . . .	71
VI. RECOMMENDATIONS . . . . .	72
Appendix	
I. CONSTANT STRESS DERIVATION . . . . .	73
II. DERIVATION OF LOAD DECREASE FOR SMALL EXTENSIONS . . . . .	78
BIBLIOGRAPHY . . . . .	81

## LIST OF TABLES

Table	Page
1. Applicable Creep Theories to a Bamboo Structured Specimen . . . . .	11
2. Activation Energy and Self-Diffusion Values for High Purity Zinc at 120°C . . . . .	17
3. Applicable Creep Theories to a Coarse-Grain Specimen . . . . .	18
4. Positions of Operation for the Creep Machine . . . . .	25
5. Linearity Data for Positions 1, 2, and 3 . . . . .	38
6. Calibration Data for Positions 1, 2, and 3 at the +0.3 Mark on Beam Position Scale . . . . .	43
7. Tensile Test Results . . . . .	49
8. Results of Creep Test A . . . . .	52
9. Results of Creep Test B . . . . .	54
10. Results of Creep Test C . . . . .	57

## LIST OF ILLUSTRATIONS

Figure	Page
1. Spectrum of Specimen Conditions According to Grain Size . . . . .	3
2. Specimen with a Bamboo Structure . . . . .	4
3. Grain Undergoing Nabarro-Herring Creep . . . . .	5
4. Movement of a Dislocation Plotted Against Time for a Pure Metal . . . . .	9
5. Simple Spring Type Constant Stress Creep Machine . . . . .	23
6. Andrade's Constant Stress Creep Machine . . . . .	23
7. Constant Stress Creep Machine Described by Andrade and Chalmers . . . . .	24
8. Constant Stress Creep Machine Described by Jackman . . . . .	24
9. Photograph of the Constant Stress Creep Machine . . . . .	26
10. Diagram of the Constant Stress Creep Machine . . . . .	28
11. Photograph of the Specimen Extension Linkage . . . . .	30
12. Diagram of the Specimen Extension Linkage . . . . .	31
13. Diagram of the Specimen Grips Drawn to Size . . . . .	32
14. Graph of Linearity Data for Position 1 . . . . .	39
15. Graph of Linearity Data for Position 2 . . . . .	39
16. Graph of Linearity Data for Position 3 . . . . .	40
17. Calibration Curve for Position 1 . . . . .	43
18. Calibration Curve for Position 2 . . . . .	44
19. Calibration Curve for Position 3 . . . . .	45
20. Typical Creep Curve for High Purity Zinc . . . . .	51

## LIST OF ILLUSTRATIONS (Continued)

Figure	Page
21. Steady State Strain Rate Versus Average Grain Size for Test A . . . . .	53
22. Steady State Strain Rate Versus Average Grain Size for Test B . . . . .	55
23. Steady State Strain Rate Versus Mean Grain Intercept for Test C. . . . .	58
24. Photograph of the Zinc Metal as Received . . . . .	60
25. Photograph of the Microstructure of Specimens after Swaging . . . . .	61
26. Photograph of the Microstructure of Bamboo Specimens . .	62
27. Photograph of the Microstructure of a Coarse-Grain Polycrystalline Specimen . . . . .	63
28. A. Photograph of a Typical Specimen Strained to Fracture in a Tensile Test . . . . .	65
B. Photograph of a Typical Bamboo Specimen Strained in Creep Testing . . . . .	65
29. Photograph of the Necked Area of a Bamboo Specimen After a Creep Test . . . . .	66
30. Photograph of the Cross Section of a Coarse-Grain Polycrystalline Specimen After Creep Testing . . . . .	68

## SUMMARY

The phenomenon of a metal elongating to 1000 percent or more, known as superplasticity, has only recently been investigated. It has been shown that the deformation of a superplastic metal can be described by available creep theories. This thesis proposed to investigate the creep of a known superplastic material and allow the grain size to vary in the coarse grain size range, in order to determine which available theory would describe the deformation. The material chosen for the investigation is high purity zinc.

A constant stress creep machine was designed and constructed, since it was necessary to hold stress constant in the study. Bamboo structured and coarse-grain polycrystalline specimens were fabricated with varying large grain sizes. Creep tests were conducted holding stress and temperature constant while monitoring strain rate.

For the bamboo structured specimens, results showed an indeterminate correlation between grain size and strain rate because localized necking of select grains of the specimens occurred. A linear relationship between grain size and strain rate was found for coarse-grain polycrystalline specimens. This linear relationship between strain rate and grain size does not agree with any of the common theories for creep.

## CHAPTER I

## INTRODUCTION

Significance of the Investigation

An efficient way to commercially apply a phenomenon is to have its theory known first. But contrary to the general opinion, this is seldom the case with materials of construction. Glass was in use for three millenia before its structure was even vaguely known. Also, martensite was used long before its mechanism was known and Duralumin was used almost a decade before the rudiments of its theory were developed. The phenomenon of a metal plastically deforming to elongations of 1000 percent or more, known as superplasticity, falls into this category. Its application to current industrial metal forming problems has received much attention while the theory of the phenomenon is being formulated simultaneously.

In 1920, Rosenhain [1]\* observed a molten glass-like behavior in a cold rolled zinc-copper-aluminum ternary alloy. Few other reports of great plastic deformations are recorded until Pearson [2] reported an amazing 2000 percent elongation in a tin-bismuth eutectic alloy in 1934. Such reports went unnoticed until 1962, when a review [3] of previous experiments by industry resulted in research and development of the phenomenon [4,5,6,7,8,9,10,11]. Currently, several aerospace companies are developing superplastic vacuum forming

\*Numbers in [ ] refer to references listed in the Bibliography.

and high ductility forging processes for use in manufacturing of parts peculiar to that industry [4,7]. Also, the automobile industry is investigating superplastic forming of sheet metals for use in car bodies [4,5]. At the same time, a theory of plasticity is being developed to model the phenomenon. The most recent of the theoretical works by Hayden, Floreen, and Goodell [12] has applied creep theories to model superplasticity. This model is in good agreement with metallographic investigations by Nicholson [13]. However, quantitative measurements concerning deformation mechanisms of only a few superplastic materials has been reported in the literature, and no single theory can account for the differences observed in them.

Pure zinc (99.99%), as well as zinc of commercial purity, has been reported to be a superplastic metal [4,8]. Investigations into single crystal creep properties [14,15,16,17,39] has been rather extensive, while the polycrystalline state [18,19,30] has received little attention. It is expected that the creep of polycrystalline zinc would be satisfactorily explained by one of the recognized creep theories that are available. The objective of the present investigation is to study the creep properties of polycrystalline zinc, in order to determine which theoretical model best fits the creep behavior for large grain sizes. The grain sizes in this investigation are larger than the range in which the material behaves in a superplastic manner. Since this investigation is concerned with the deformation of zinc occurring under conditions of steady state creep, a review of applicable deformation theories found in the

literature is in order.

### Review of Theories of Steady State Creep

#### Classification of Specimens

With respect to the crystal size, Figure 1 shows the spectrum of possible states into which a specimen of metal may be classified. This classification scheme makes use of the assumption that the specimen has a circular cross section, i. e., in the form of wire or rod. For purposes of this investigation, it is necessary to consider those creep theories which are applicable to the so-called "bamboo" and coarse-grain specimens.

Consider the cylindrical specimen in the diagram of Figure 2, which represents a test specimen with large crystals stacked end to end. The ratio of the grain diameter to the specimen diameter is equal to one, and the crystals are equally spaced along the length of the specimen. This represents a specimen with the bamboo structure. Several creep theories are available to explain the plastic deformation of such a specimen.

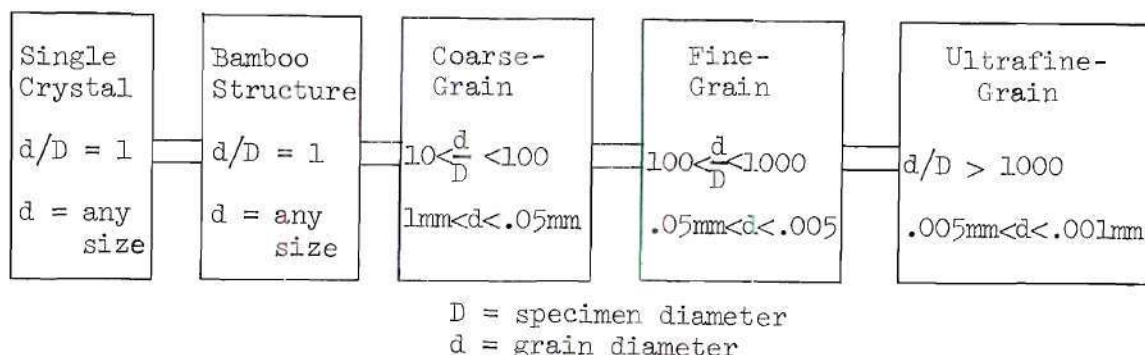


Figure 1. Spectrum of Specimen Conditions According to Grain Size.



Figure 2. Specimen with Bamboo Structure.

### Herring Theory

Herring [21] and Nabarro [22] have proposed a diffusional deformation mechanism. The steady state creep rate equation that was developed is

$$\dot{\epsilon}_{ss} = \frac{\alpha \sigma D_L \Omega}{d^2 k T} \quad (1)$$

where

$\dot{\epsilon}_{ss}$  = steady state strain rate

$\alpha$  = constant

$\sigma$  = applied stress

$D_L$  = lattice diffusion coefficient

$\Omega$  = vacancy volume

$d$  = grain size

$k$  = Boltzmann's constant

$T$  = absolute temperature.

The basis for equation (1) is that any crystal can, through self-diffusion, change its shape and cause the polycrystalline aggregate to deform in a viscous manner. In the presence of an applied

stress, diffusional currents are established, as is shown in the diagram of Figure 3. This results in the diffusion of matter away from grain boundaries where there is a normal compressive stress, and toward boundaries where there is a normal tensile stress. Crystalline flow is thus accomplished by the diffusion of atoms through the lattice, with the diffusion of vacancies forming a counterflow.

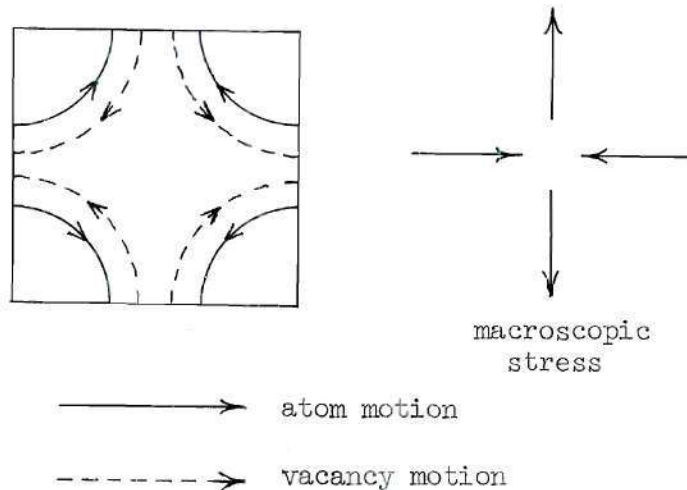


Figure 3. Grain Undergoing Nabarro-Herring Creep [34].

Additional assumptions are that the surface of the crystal is the source and sink for the vacancy gradient, the temperature must be sufficiently high such that the self-diffusion mechanism is activated, and the specimen is in an equiaxed, polycrystalline condition.

Equation (1) was modified by Herring [21] to account for the

specimen having a bamboo structure. His analysis arose in an effort to satisfactorily explain the experiments on wire specimens with a bamboo structure performed on copper by Udin, Shaler, and Wulff [23], and on pure aluminum by Dushman, Dunbar, and Huthsteiner [24]. The resulting equation is

$$\dot{\epsilon}_{ss} = \frac{\alpha \sigma D_L \Omega B}{d L k T} \quad (2)$$

where  $\alpha$ ,  $\sigma$ ,  $D_L$ ,  $\Omega$ ,  $d$ ,  $k$ , and  $T$  have the same meaning as in equation (1) and

$$B = f(d/D) = 12.3 \text{ for } d/D = 1$$

$L$  = average spacing of grains on the longitudinal axis of the specimen.

Equation (2) can be generalized for a given material. The generalized form is written

$$\dot{\epsilon}_{ss} = \frac{A \sigma}{d L T} \quad (3)$$

#### Gilman-Weertman Theory

Since the bamboo structured specimen is essentially a series of single crystals of different orientations stacked end to end, it is likely that whatever mechanism dominates the deformation of single crystals may also dominate the bamboo structure. The high purity zinc monocrystal experiments of Coffin and Weinan [15], Weinberg [16],

Miller [17], Gilman [14], and Cottrell [18] are worth examining in this respect.

The main phenomenon pointed out in these investigations is the effect of crystal orientation. The strain rate changes greatly depending on how the "c" axis (zinc has a hexagonal close packed lattice structure) is oriented with respect to the tensile axis. Zinc is an unusual metal in that at low temperatures slip can only occur on the basal plane ((0001) plane), whereas at elevated temperatures zinc is also capable of deforming through prismatic glide on the (1010) plane [14]. Deformation will occur when the critical resolved shear stress on one of these two planes is reached.

Gilman reports that at elevated temperatures, prismatic glide will be the controlling deformation mechanism rather than slip occurring along the basal plane [14]. He suggests the following equation

$$\sigma_c = K \dot{\epsilon}_{ss}^{1/3} \quad (4)$$

where

$\sigma_c$  = the critical resolved shear stress

$K$  = a temperature dependent constant.

Since only a fraction of the crystals will be oriented in a satisfactory position for glide to occur, the creep rate of a bamboo structured specimen will be only a fraction of that of the single crystal rate. Thus, for the bamboo specimen equation (4) can be

rewritten as

$$\sigma_c = KN\dot{\epsilon}_{ss}^{1/3} \quad (5)$$

where  $N$  is the fractional length of properly oriented crystals. At temperatures near half of the melting temperature, where the dominant mechanism may be basal or prismatic slip, the exponent of the steady state creep rate may change. Equation (5) can be generalized to account for this condition. Thus

$$\sigma_c = KN\dot{\epsilon}_{ss}^{1/m} \quad (6)$$

where  $m$  is a temperature dependent constant. Equation (6) is not a function of the grain size, whereas equation (3) is.

A further investigation of the theory which explains the deformation of a single crystal is in order, since  $\dot{\epsilon}_{ss}$  from equation (6) lacks satisfactory definition. Crystallographic slip is generally agreed to be a phenomenon caused by dislocation movement. McLean [25] characterized the movement of a dislocation through a pure metallic crystal by the diagram of Figure 4. For zinc, slip is the movement of dislocations in planes parallel to the basal plane. The climb of dislocations, or movement perpendicular to the glide plane, is the recovery process. (Recovery is the modification of mechanical properties of a metal and is generally considered to be the reverse of strain hardening.)

Dislocations can be the result of crystalline imperfections, grain boundary irregularities, or can be generated under an applied stress through operation of Frank-Read sources, Weertman mechanisms [34], etc. They move through the lattice impeded only by stress

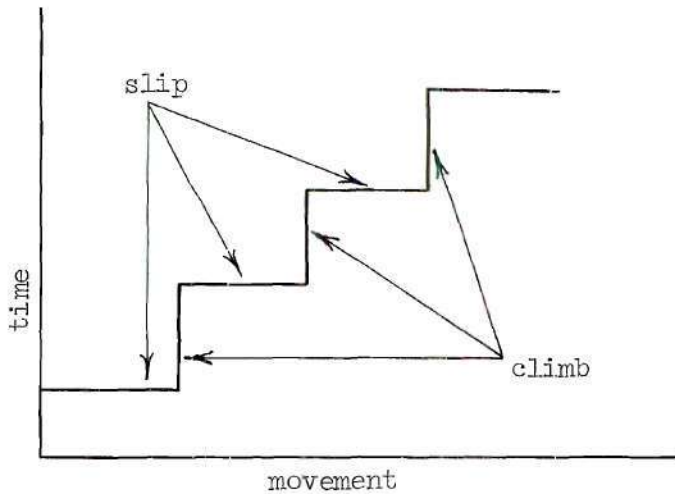


Figure 4. Movement of a Dislocation Plotted Against Time for a Pure Metal.

fields of other dislocations, boundaries, and impurities [40]. The crystal will experience a decrease in deformation rate when dislocations no longer move because of annihilation (eg., uniting of two screw dislocations of opposite sign), or dislocation pile up and immobilization by some obstacle. This is the work hardening process. Steady state creep occurs when the work hardening of the material is completely

balanced by recovery.

Weertman [25] has suggested a mechanism to explain the gliding and climb of dislocations as is applicable to single crystal deformation. His analysis assumes that dislocations are created at Frank-Read sources and move at a rate governed by the force exerted on the crystal. The analysis results in the creep rate equation

$$\dot{\epsilon}_{ss} = \frac{3b^2}{\mu AB} \quad (7)$$

where

$b$  = Burgers vector length

$\mu$  = shear modulus

$A$  = temperature dependent constant

$B = \mu b^2 / 2\pi(1 - \nu)$ .

Equation (7) satisfies the third power stress dependence observed by Gilman [14] (equation (4)). Weertman [26] also proposed another analysis. In it he assumes that the rate controlling mechanism is the frictional resistance to motion that a dislocation must overcome, i. e., the Peierls force. This yields an identical equation except the exponent on the applied stress,  $\sigma$ , is equal to 2.5 for low stresses. It can be seen that for a given material, Weertman's analyses show that the creep rate is not dependent on the grain size.

The following table, Table 1, summarizes the preceding discussion concerning the theories of creep which are applicable to describing the deformation of a specimen with a bamboo structure.

Table 1. Applicable Creep Theories to a Bamboo Structured Specimen.

Theory	Generalized Strain Rate Equation	Grain Size Dependence	Stress Dependence
Herring	$\dot{\epsilon}_{ss} = \frac{A\sigma}{dLT}$	1/d, 1/L	$\sigma$
Weertman-Gilman	$\dot{\epsilon}_{ss} = B\left(\frac{\sigma}{N}\right)^n$	independent	$\sigma^n$ $2.5 < n < 3.0$

### Nabarro Theory

The following discussion is concerned with those creep theories which are applicable to specimens with a coarse-grain polycrystalline structure.

Nabarro [26] has modified his original diffusional creep theory to include a material with large grains. Once again, the assumption of his vacancy diffusion model is that under an applied stress, atoms will flow to relieve the stress, and vacancies will form a counter-flow. In his revised theory the sources and sinks for the vacancy gradient are no longer the grain boundary, but are dislocations in the crystal (which is perhaps an oversight in Herring's development of generalized equation (3)). His original theory was developed for fine-grain materials, where the large grain boundary area was a sufficient source. In a coarse-grain material this is not the case.

Nabarro [27] proposes two theories based on the preceding assumption. The first is for medium to high temperatures, where self-diffusion of atoms through the lattice is possible. The second is for lower temperatures where diffusion of atoms and vacancies occurs along grain boundaries. We need only consider the first case.

The equation given by Nabarro for medium to high temperatures is

$$\dot{\epsilon}_{ss} = \frac{\pi F \Omega}{d^2} \quad (8)$$

where

$$F = \frac{D \sigma}{\frac{L}{2} k T} / \nu \frac{4G}{\pi \sigma}$$

and G is the shear modulus, and all other symbols have the same meaning as in equation (1). In the case of lower temperatures, the exponent of the applied stress changes. Generalizing equation (8), as has been done in previous creep rate equations, produces

$$\dot{\epsilon}_{ss} = \frac{C \sigma^n}{d^2 T} \quad (9)$$

where C is a constant.

#### Kosevich-Saralidze-Slezov Theory

Kosevich, et al. [28], have proposed a diffusion mechanism of

deformation similar to that of Nabarro [27], with quite different results. Once again, the sources and sinks of vacancies are dislocations, and in particular, are prismatic dislocation loops within the grain. A prismatic dislocation loop is simply a loop containing mostly edge dislocations whose slip planes intersect in parallel lines and thus form a prism or cylinder. In essence, the prismatic loop is a congregation of vacancies. The resulting creep rate equation can be written

$$\dot{\epsilon}_{ss} = \frac{D_L n \sigma w d^2}{\lambda_0 k T} \quad (10)$$

where

w = the atomic volume

$\lambda_0$  = the radius of an average dislocation loop

n = the vector normal to the dislocation vector

and all other symbols have their usual meaning.

The most striking feature of this theory is that the creep rate is proportional to the square of the grain size. Generalizing equation (10), for a given material yields

$$\dot{\epsilon}_{ss} = \frac{P \sigma d^2}{T} \quad (11)$$

where P is a constant.

#### Coble Theory

In an effort to explain the creep observed in polycrystalline

alumina, Coble [29] has proposed a theory, which is based on boundary diffusion rather than lattice diffusion, as in the theory of Nabarro-Herring. The theory is satisfied over a wide range of temperatures and stresses, whereas the Nabarro theory is best suited for high temperatures and low stresses. Coble suggests that boundary diffusion is rate controlling when grains are large.

The Coble theory is based on a model of the crystal that is equiaxed and spherical in shape. The driving force, as in the theory of Nabarro-Herring [21], is a concentration gradient of vacancies moving under an applied stress. Vacancies do not move through the lattice, but move only along the boundary, and the boundary imperfections are the sinks and sources of vacancies. In addition to deformation by diffusion, Coble also proposes that the deformation rate can be increased by shear stress relaxation at boundaries undergoing changes in shape. The result of the analysis is given by equation (12) and generalized for a given material in equation (13).

$$\dot{\epsilon}_{ss} = \frac{148 D_b w a^3}{d^3 k T} \quad (12)$$

where

$D_b$  = diffusion coefficient for atoms in the boundary

$w$  = effective boundary width

$a$  = atomic volume

and all other symbols have their usual meaning.

$$\dot{\epsilon}_{ss} = \frac{R\sigma}{d^3 T} \quad (13)$$

where  $R$  is a constant. Thus, for this theory, the steady state strain rate is inversely proportional to the cube of the grain size.

#### Grain Boundary Sliding

Evidence of grain boundary sliding has been produced by metallographic examinations of pure polycrystalline zinc samples deformed at constant stress by Cottrell and Aytekin [18], and McLean and Farmer [30]. For fine grain specimens ( $d \approx 0.25$  mm.) tested at  $150^{\circ}\text{C}$  and stresses of approximately 1000 psi., it was found that the amount of deformation contributed to the total by grain boundary sliding was 77 percent and remained relatively constant throughout higher temperature ranges.

Stevens [32,33] points out that as grains become large and test temperatures drop below  $0.5 T_m$  of a given metal, that grain boundary sliding is no longer an important deformation mechanism. The value of the contribution of grain boundary sliding to the total deformation drops to about 10 percent for fine grain specimens and continues to diminish for large grain specimens according to the expression

$$\dot{\epsilon}_{GB} = K N \bar{X} \quad (14)$$

where

$K$  = constant

$\bar{X}$  = average displacement of a grain boundary

$N$  = average number of grain boundaries per unit length.

Where grains are large, the value of  $N$  is small and the amount of strain that can be attributed to grain boundary sliding is minimized. Therefore, in coarse-grain specimens, grain boundary sliding is not a prominent deformation mechanism [32].

#### Dislocation Theory

Weertman [34,35,36] has proposed several theories based on dislocation movement which predict strain rates of polycrystalline materials tested under a variety of conditions. These are all based on dislocation climb being rate controlling. He states that for hexagonal close packed metals like zinc, dislocation climb may not be rate controlling, since dislocation glide takes place with comparative ease (refer to discussion concerning equation (7)).

In the event that dislocation climb is rate controlling, the expression for the steady state creep rate is given by

$$\dot{\epsilon}_{ss} = \frac{K \sigma^n e^{-Q/kT}}{kT} \quad (15)$$

where

$K$  = constant

$Q$  = activation energy of steady state creep

$n$  = constant,  $3 < n < 4$

Equation (15) is independent of grain size.

The derivation of equation (15) is based on the assumption that the activation energy of steady state creep equals that of self-

diffusion. The values of these parameters are given by Dorn [37], and Cottrell and Aytekin [18], and can be compared in Table 2. At 120°C the value of the activation energy for steady state creep is much less than that of self-diffusion, and thus the mechanism described by equation (15) may not be operational. It would become operational at a much higher temperature.

Table 2. Activation Energy and Self-Diffusion Values for High Purity Zinc at 120°C [18,37].

	$Q$ Activation Energy in cal/mole	$D$ Self-Diffusion Coefficient in cal/mole
Single Crystal	28,000-30,000	22,000-30,000
Polycrystal	11,000-13,000	22,000-23,000

Equation (7) has been modified by Weertman [34] to include the conditions of dislocation glide being rate controlling in a polycrystalline specimen. He presents a strain rate equation similar to equation (15), which is also independent of grain size. Furthermore, Dorn [38] has suggested a relationship based on the movement of jogged screw dislocations, which is also independent of grain size.

The following table, Table 3, served to summarize the preceding discussion about applicable deformation mechanisms to the creep of coarse-grain zinc specimens.

Table 3. Applicable Creep Theories to a Coarse-Grain Specimen.

Theory	Generalized Strain Rate Equation	Grain Size Dependence	Stress Dependence
Nabarro	$\dot{\epsilon}_{ss} = \frac{C\sigma^n}{d^2 T}$	$1/d^2$	$\sigma^n$
			$1 < n < 2$
Kosevich, et al.	$\dot{\epsilon}_{ss} = \frac{P\sigma d^2}{T}$	$d^2$	$\sigma$
Coble	$\dot{\epsilon}_{ss} = \frac{R\sigma}{d^3 T}$	$1/d^3$	$\sigma$
Weertman, et al.	$\dot{\epsilon}_{ss} = \frac{S\sigma^n}{T}$	independent	$\sigma^n$
			$3 < n < 4$

Statement of the Problem and Attack

The purpose of this investigation is to determine how the creep rate of high purity zinc depends on the grain size. As is shown in

the previously discussed theories of creep, if temperature and stress are held constant, the steady state strain rate depends solely on the grain size according to

$$\dot{\epsilon}_{ss} = \frac{K}{d^n} \quad (15)$$

where

$K$  = a constant

$d$  = the grain size, and

$n$  is to be experimentally determined.

A comparison between the experimental value of  $n$  and its theoretical values provides a basis for determination of the primary deformation mechanism.

The investigation is carried out in the following manner:

- (1) A constant stress creep apparatus is designed and constructed.
- (2) Specimens of high purity zinc with varying grain sizes are tested on the apparatus, holding stress and temperature constant ( $20^{\circ}\text{C}$ ). Deformation rate data is taken and analyzed.
- (3) A microscopic evaluation of specimen microstructure before and after testing is done to verify the results of mechanical testing.

In addition, the effect of the number of crystals in the cross section of a specimen is to be investigated (bamboo as opposed to a coarse-grain polycrystalline specimen deformation). This is

done by using two different sizes of specimens with different microstructures. It was expected that the effects of crystal orientation would appear in test results with bamboo specimens, whereas these effects would be negligible in a polycrystal aggregate. The grain size dependence of strain rate could thus change and a different deformation mechanism would be indicated.

## CHAPTER II

## EXPERIMENTAL APPARATUS, MATERIAL, AND PROCEDURE

A creep machine was designed and constructed specifically for use in this investigation. The machine differs from the usual constant load type creep machines in that the load varies in such a manner that a constant stress is applied to the test specimen. The rationale behind constructing such a device was twofold. First, the theories of deformation that are under investigation are described by equations in which stress is a variable. Since it was necessary to hold stress constant in the investigation, constant load or variable stress creep machines would be inapplicable. Though for small elongations the condition of constant stress is approximated by the constant load creep machine, Cottrell and Aytekin [18] report that for zinc, a small change in stress level can produce large changes in strain rate (even for strains of less than 1 percent). An added feature of the constant stress creep machine is that it is the apparatus that is conveniently used for temperature activation studies and further investigations of creep associated phenomena.

Review of Constant Stress Creep Machines

There are several methods by which one may vary the load input to a test specimen in tension such that constant stress is achieved. One way would be to employ a spring system in association with a constant load creep apparatus such that as a specimen elongates,

the load would be relieved by the spring system. The diagram of Figure 5 shows such a simple machine. The choice of the spring in such a system, however, is rather difficult, and the construction of such a system is therefore not considered.

Andrade [20] proposed a second method, shown in the diagram of Figure 6. The sides of the load weight are hyperbolic and the weight is partially immersed in water. As the specimen extends, the load on the specimen decreases as the load weight is buoyed by the water. Such a system was considered impractical for this investigation.

Andrade and Chalmers [20] described a third constant stress creep machine. It is shown in the diagram of Figure 7. The load beam plates B and C are made such that the moment of the load about A varies with the tilt of the beam inversely as the length of the specimen under test.

A fourth method, described by Jackman [41], is utilized in this investigation, because it has a greater versatility than any of the other systems. Referring to Figure 8, it can be seen that as the specimen elongates, the moment of the load taken about the fulcrum of the lever decreases as the right angle loading beam swings toward the fulcrum. The effective load applied to the specimen therefore decreases. The beam maintains constant stress because the decrease in the diameter of the specimen as it elongates during creep is offset by an accompanying decrease in load produced by the movement of the load arm. The length of the specimen,  $\ell$ , and  $L_1$ ,  $L_2$ , and  $L_3$  must be so chosen that the correct movement occurs. A derivation of

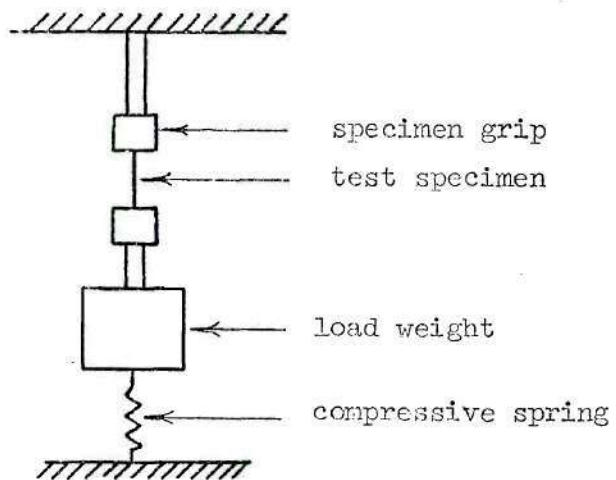


Figure 5. Simple Spring Type Constant Stress Creep Machine.

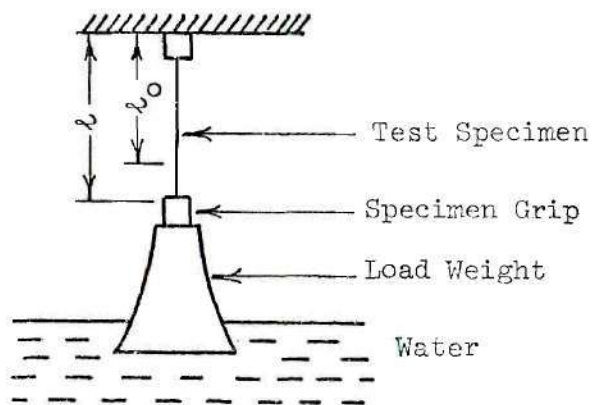


Figure 6. Andrade's Constant Stress Creep Machine.

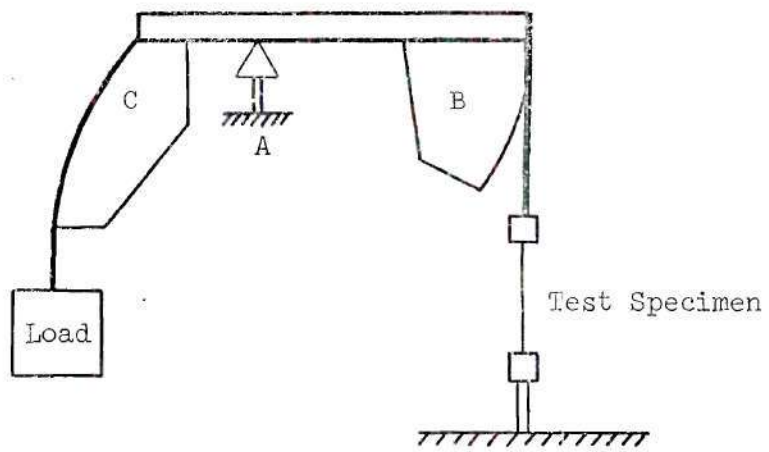


Figure 7. Constant Stress Creep Machine Described by Andrade and Chalmers

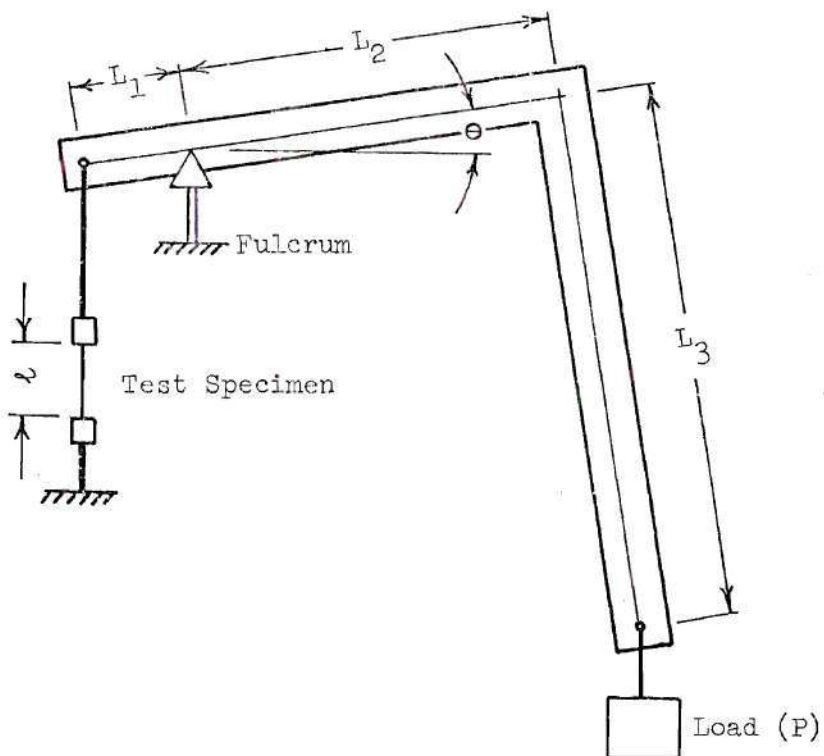


Figure 8. Constant Stress Creep Machine Described by Jackman.

the relationship that the lengths must follow is shown in the Appendix I. That relationship is

$$\ell = \frac{L_2 L_1}{L_3} \quad (16)$$

Choice of the various lengths was made according to the following criteria. The specimens to be tested were to be made into wire or small diameter rod. The gauge lengths ( $\ell$ ) were to be two and three inches. Stress input to the specimens was to be in the range of 100 to 100,000 psi. These specifications allow a wide range of materials to be tested at a variety of stresses.

Table 4 shows the various lengths that were chosen for the design of the creep machine.

Table 4. Positions of Operation for the Creep Machine

Position	$\ell$	$L_1$	$L_2$	$L_3$
1	3.0	6.0	24.0	48.0
2	3.0	3.0	24.0	24.0
3	2.0	3.0	24.0	36.0

#### General Description of the Creep Machine

The creep machine with a specimen under test can be seen in the photograph of Figure 9 and in the diagram of Figure 10. The frame

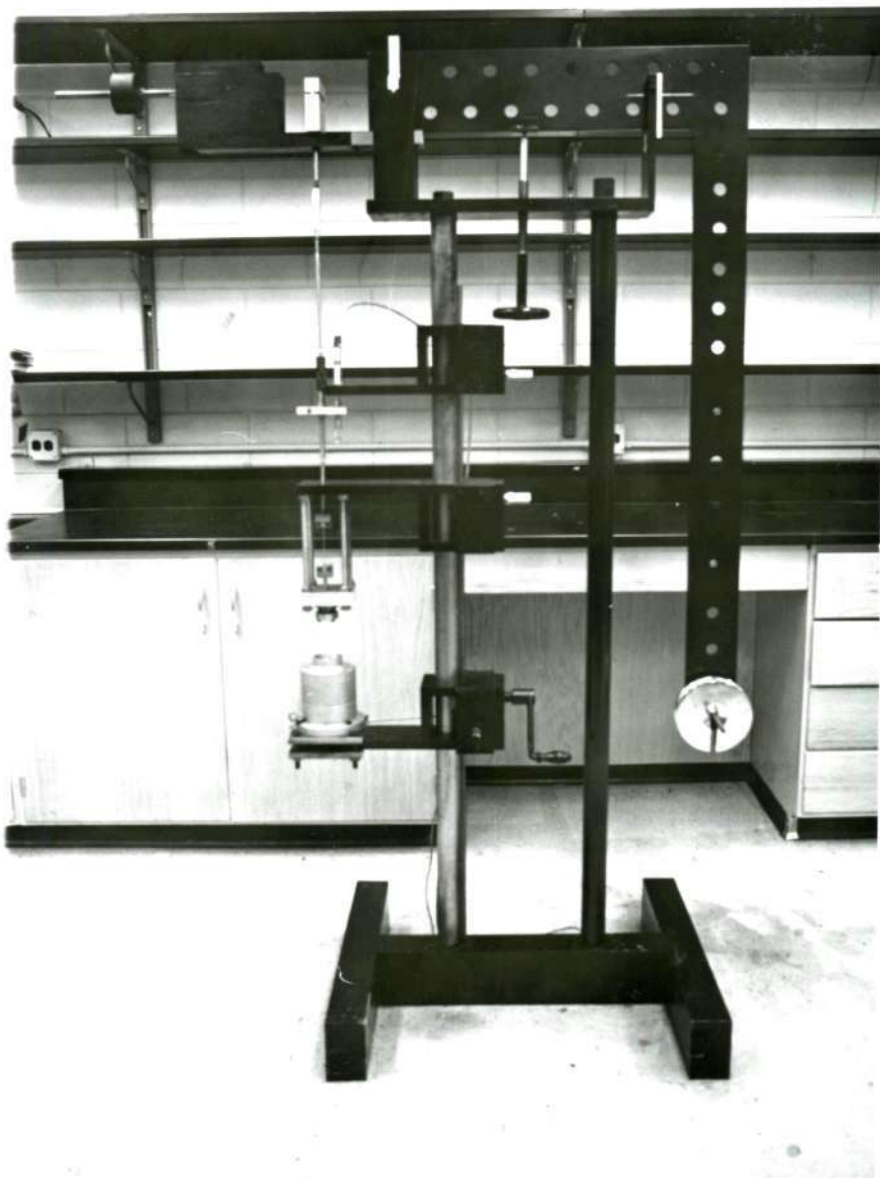


Figure 9. Photograph of the Constant Stress Creep Machine.

Key for Figure 10

1. creep machine base
2. support column
3. transducer holding cradle
4. specimen holding cradle
5. load cell cradle
6. specimen grips
7. specimen
8. ball and socket joint
9. extension platform
10. micrometer head
11. universal joint
12. turnbuckle
13. counterbalance weights
14. specimen extension linkage knife edges
15. load arm knife edges (fulcrum)
16. beam support
17. deformation transducer
18. beam position scale
19. horizontal position mark
20. load arm
21. load placement, position 3
22. load placement, position 2
23. load placement, position 1
24. load weight
25. top base
26. specimen base
27. weight holding rod
28. load cell

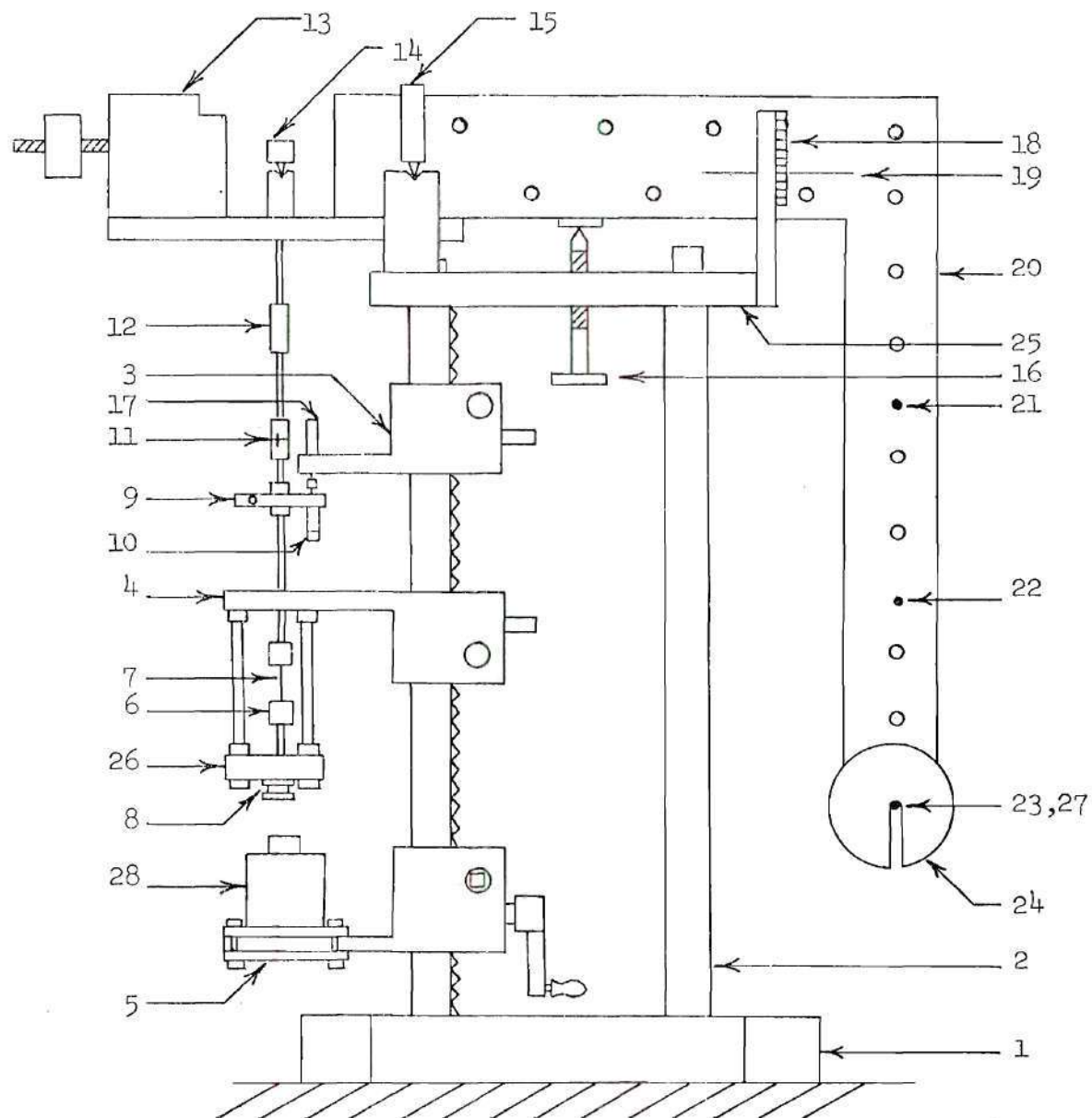


Figure 10. Diagram of Constant Stress Creep Machine.

of the machine consists of two 2-inch diameter columns (2)\* mounted to a heavy steel base (1), and bolted to an inch thick steel top base (25). The left column has a rack gear mounted to it, which facilitates movement of the cradles (3,4,5) up and down the column by means of a rack and pinion gear system.

The cradles (3,4,5) hold the deformation measuring transducer (17), specimen (7), and load cell (28), respectively.

The cradles are made in a massive box type construction, largely of 3/4-inch by 4-inch cold rolled steel plate. Each cradle is fitted with a brass brake for holding the cradle in position on the column.

The specimen (7) is held by means of grips fabricated from stainless steel, and is put into tension by means of a linkage, which is more easily seen in the schematic of Figure 12 and the photograph of Figure 11. A diagram showing the details of the specimen grips is shown in Figure 13. A diametrical interference fit of .004 inch was used to hold the specimen during creep testing.

The specimen extension linkages are made of 1/4-inch diameter cold rolled steel. The universal joint (11) and the ball and socket joint (8) are employed in the extension system to assure that the specimen is put in uniaxial tension. A balanced extension platform (9) holding a micrometer head (10) along with the deformation measuring transducer (17) and its amplification and readout devices allow monitoring and measurement of the deformation of the specimen. The

\*Numbers in ( ) indicates parts of the machine as per Figure 10.

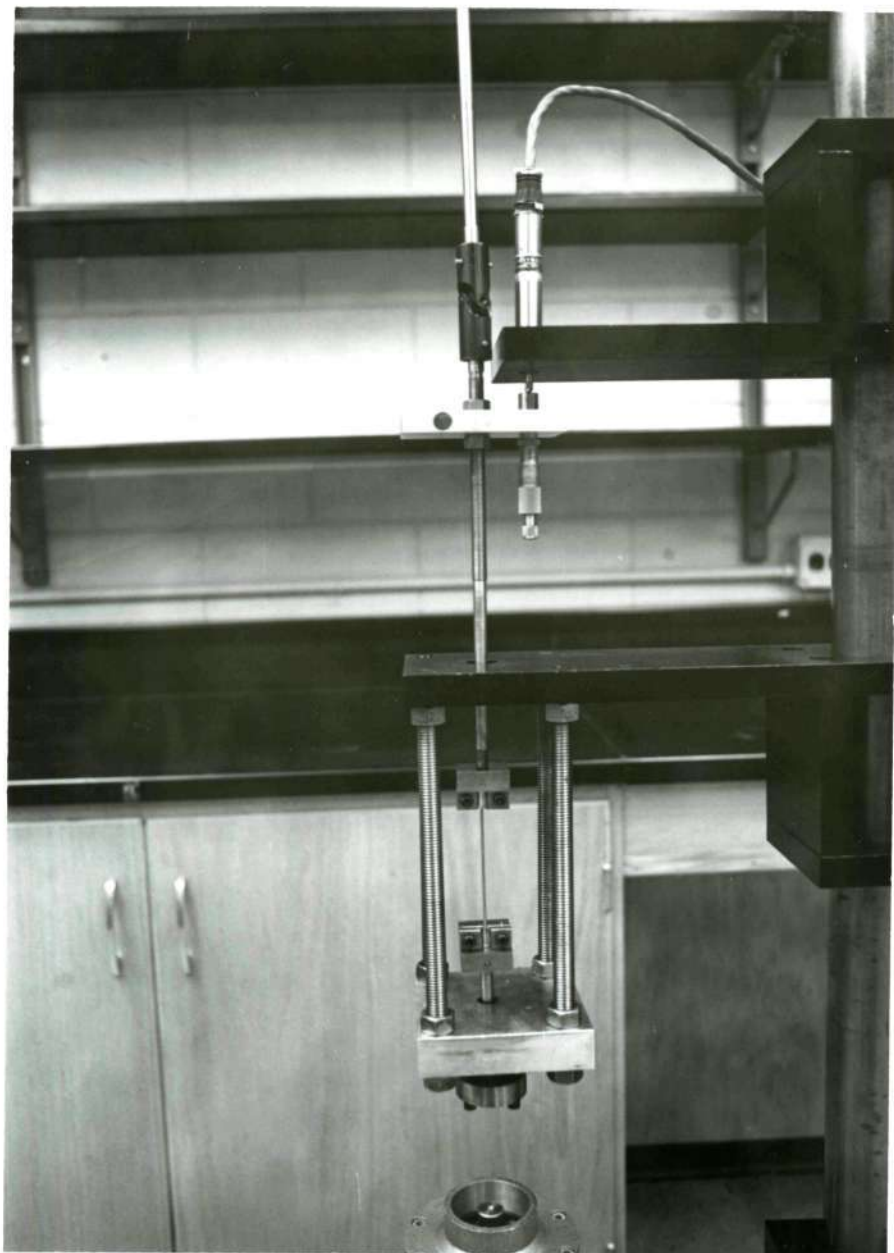


Figure 11. Photograph of the Specimen Extension Linkage.

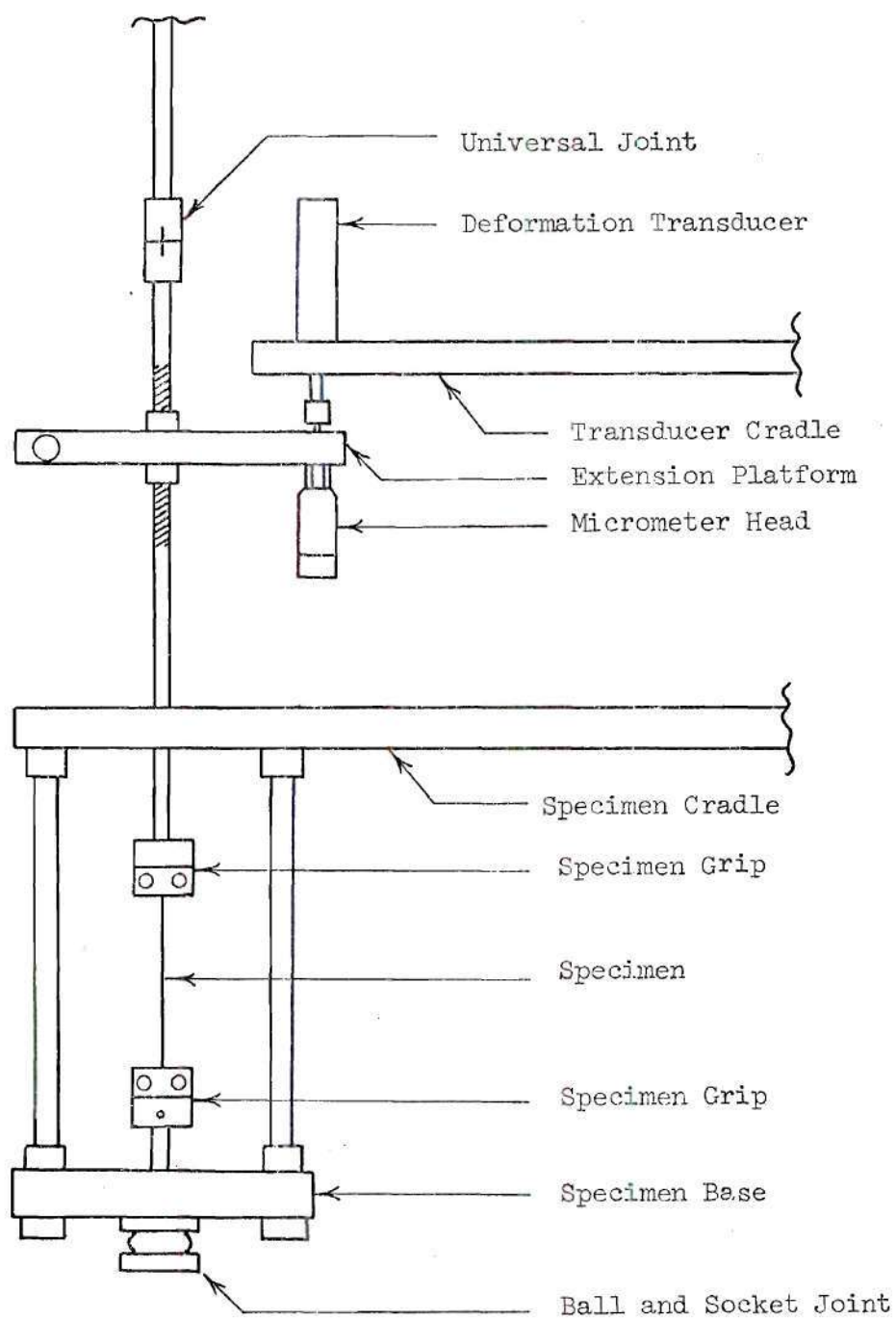


Figure 12. Diagram of the Specimen Extension Linkage.

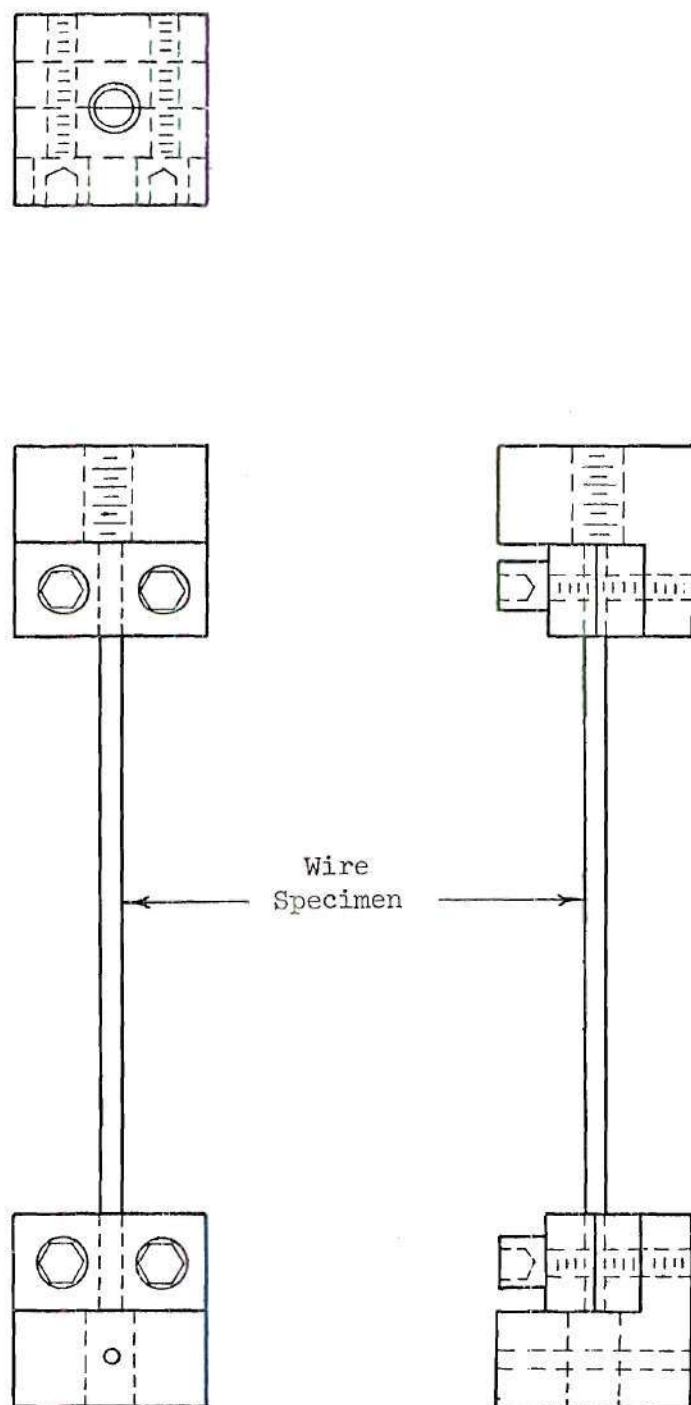


Figure 13. Diagram of Specimen Grips Drawn to Size.

micrometer head is necessary since the zero position of the particular transducer that was used is in the middle of its 0.2 inch total travel. The zero point must be located at the beginning of each test using the micrometer head. The specimen is held beneath the specimen holding cradle by means of four threaded stainless steel rods holding a one inch thick aluminum specimen mounting base (26), to which the specimen is fixed by means of a ball and socket joint. Completing the specimen extension linkage is a turn-buckle (12) for eliminating slack in the linkage and a set of knife edges and holders (14).

There are two sets of knife edges in the total loading system. They are made of Rex MM tool steel hardened to  $65 R_c$ . Knife edges are employed in the system at crucial bearing points to reduce friction. The bearing points are also lubricated with a light machine oil.

Since the load arm is to be balanced before a load is input to the test specimen, the arm is fitted with counter balance weights (13). The weights can be adjusted such that the beam is in balance about the fulcrum (load arm knife edges (15)) and is also balanced across the centerline of the beam. The load arm itself is fabricated out of 1/2-inch thick 2024 aluminum plate. Aluminum was chosen as the material for the load arm because it is light and strong. The need for a light beam arises, since a heavier load arm would necessitate a more massive counterbalance system, and it is desirable to keep the total mass of the system minimal such that load input sensitivity is maximized.

Of special note is the beam position scale (18) and the

horizontal position mark (19) scribed on the load arm. The fact that the beam will produce constant stress is based on the assumption that beam movements are small and are about this centerline. Tests run to calibrate the machine show that the machine can operate as predicted by theory from a maximum displacement of  $\pm 0.3$  inches from the horizontal position on the scale (refer to Calibration section). The use of the scale and the beam support (16) allow proper positioning of the beam such that the machine will operate as designed.

There are three positions that the load weight (24) can be applied, as is noted in Table 4 ( $L_3$  assumes three different values). These positions are marked as numbers 21, 22, and 23 on Figure 10. The rod holding the weight extends on both sides of the load arm and is designed to hold Instron Tensile Test Machine calibration weights. Weight is to be uniformly applied across the beam so as to avoid creating a moment at the fulcrum knife edge (15).

The transducer employed in this investigation is the Daytronic model DS-200 and has a linear range of  $\pm 0.1$  inch. It is a linear variable differential transformer type transducer with a movable core which rests against the micrometer head in the specimen extension linkage. With this arrangement, as the specimen extends the relative displacement of the two specimen grips is detected by the transducer. This motion is translated into an electrical signal which is amplified by a Daytronic model 300D Transducer Amplifier Indicator with a Type 73 Differential Transformer Plug-in-Unit. This transducer-amplifier system is capable of measuring a displacement of .00001 inch. In

order to establish a permanent record of the displacement during a creep test, the output of the Daytronic amplifier was input to a Leeds and Northrup Speedomax H strip chart recorder. The chart operates at a constant five minutes per inch of chart. This slow chart recording speed was necessary as the duration of the creep tests was to be at least two hours.

#### Testing of the Apparatus

A variety of tests were performed on the machine elements to determine that they would function as designed. The machine was also calibrated for its three positions of operation and a series of tests run to determine that the machine would, in fact, act to reduce the load input to the test specimen at the necessary rate in order to produce constant stress.

The first test performed was a calibration of the transducer-amplifier-recorder system. An Instron Calibration Micrometer, reading accurately to 0.0001 inch was used to mechanically simulate a displacement, from which the rest of the elements were calibrated. This calibration test showed that the displacement measuring system has a sensitivity of 0.00001 inch. Recalibration of the system was also performed at the start of each day of testing to assure proper operation of these elements.

A test was performed to test for creep of the specimen extension linkages. A dummy specimen was fabricated from cold rolled steel, the same material as the linkages are made from. This was inserted into the system using the specimen grips and linkages, and then put

under a stress of approximately 3000 psi. (40 lbs. input). The displacement measuring system was used to detect any movement or creep in the linkages. An elastic deflection of linkage elements was observed but no creep of the linkage elements was observed over a two hour period.

A test was performed to check for cradle movement. The cradles were braked properly, then subjected to severe hammering, which resulted in no cradle movement.

The creep tests were to cover, at a maximum, 0.2 inch of specimen extension as is allowed by the transducer operation range. It was necessary to determine if the machine would produce a constant stress over this extension range. The derivation in Appendix II shows that for small extensions of a specimen undergoing uniform elongation, that in order to maintain a constant stress, the load must decrease linearly. The rate of decrease is given by

$$P_2 = \frac{P_1 \ell_1}{\ell_2} \quad (17)$$

where

$P$  = the load

$\ell$  = specimen length.

The subscripts indicate two points in time during the creep test. It is seen that the ratio of  $\ell_1/\ell_2$  dictates how the load must decrease.

From this it was calculated that the linear reduction in load for a three inch gauge length specimen is 3.3 percent and for a two

inch gauge length specimen, it is 4.8 percent, for a 0.1 inch extension.

In order to check to see if the machine was operating in this manner, an Instron D type cell (28) was connected to the extension system and a simulated specimen extension was conducted for the three load placement positions, while monitoring the load on the specimen and inputting 10 pounds on the load arm. The results can be found in Table 5, and the proper linearity seen in the graphs of Figures 14, 15, and 16.

In each case the load decreases linearly for beam positions of approximately  $\pm 0.3$  inches from the horizontal, which exceed the necessary beam position for a 0.2 inch specimen elongation. The percent decrease in load was calculated to be 3.7 percent, 4.0 percent, and 4.3 percent for positions 1, 2, and 3 respectively. Therefore, the maximum error induced by the machine is a 0.8 percent error in load input for a maximum specimen extension of 0.2 inch. The agreement between predicted and experimental load decrease is good and the machine was therefore determined to be in satisfactory operating order.

Since the starting point for all creep tests was determined to be at the 0.3 mark on the beam indication scale from the preceding test, it was necessary to determine what load input at the three loading positions would produce what load output on the test specimen.

Again, the Instron D Load Cell was used to determine this experimentally, by employing it in the extension system as before.

Table 5. Linearity Data for Positions 1, 2, and 3.

Position on Beam Scale	Load on Specimen Position 1 - lbs.	Load on Specimen Position 2 - lbs.	Load on Specimen Position 3 - lbs.
+0.5	43.0	84.0	84.5
+0.4	41.5	82.2	83.2
+0.3	40.5	81.2	82.0
+0.2	40.0	80.2	81.0
+0.1	39.5	79.2	79.8
0.0	39.0	78.0	78.5
-0.1	38.5	77.0	77.5
-0.2	37.7	76.0	76.5
-0.3	37.0	75.0	76.0
-0.4	36.2	73.7	75.0
-0.5	34.5	72.5	73.5

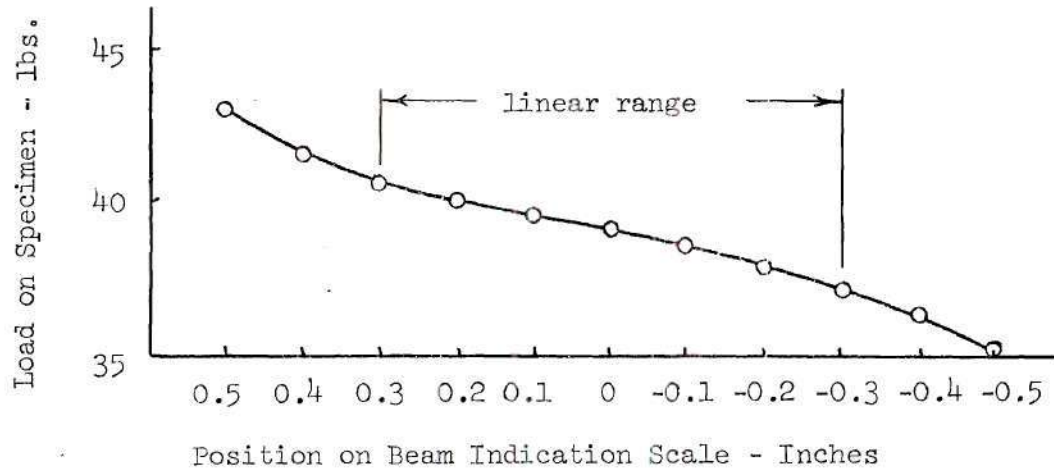


Figure 14. Graph of Linearity Data for Position 1.

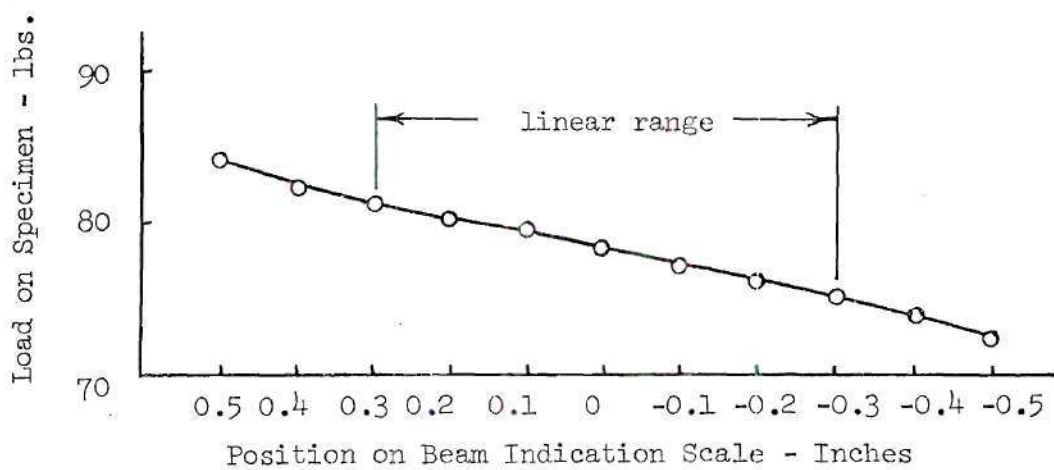


Figure 15. Graph of Linearity Data for Position 2.

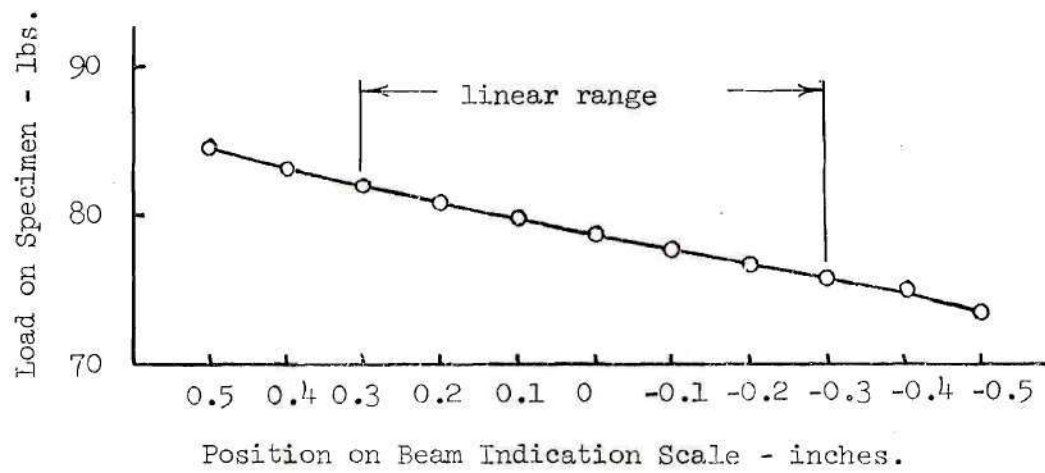


Figure 16. Graph of Linearity Data for Position 3.

The results of this testing can be found in Table 6 and the graphs of Figures 17, 18, and 19.

#### Specimen Preparation

The metal used in this investigation was 99.99+ percent pure zinc, prepared by the New Jersey Zinc Company. An analysis of impurities content given by them is as follows:

Zinc content.....	99.99+%
Lead.....	0.003% maximum
Iron.....	0.001% maximum
Cadmium.....	0.003% maximum
Tin.....	0.0005% maximum

High purity zinc has a number of advantages over other materials that could have been used in this investigation. It is a known superplastic metal that creeps and exhibits extended plasticity at room temperature. Since the use of coarse-grain specimens was necessary, zinc is an excellent metal to use because crystals are easily grown by the strain-anneal method to a larger size. Zinc also creeps at low stresses thus allowing larger diameter wires to be tested without applying excessive loads.

The zinc was received in the form of 12 inch long, 3/8-inch diameter cast rods. The microstructure of the material as received can be seen in the photograph of Figure 24. The surface impurities were removed from the rods using 400 grit abrasive paper followed by macroetching in a solution of 50 percent nitric acid ( $\text{HNO}_3$ ) and distilled water. The rods were then swaged down to the desired diameter (refer to individual tests). The microstructure of the swaged material can be seen in the photograph of Figure 25. After

Table 6. Calibration Data for Positions 1, 2, and 3 at the +0.3 Mark on Beam Position Scale.

Load Input lbs.	Load on Specimen Position 1 - lbs.	Load on Specimen Position 2 - lbs.	Load on Specimen Position 3 - lbs.
0.0	0.0	0.0	0.0
1.0	4.1	8.2	8.1
2.0	8.15	16.3	16.2
3.0	12.2	24.5	24.5
4.0	16.5	32.7	32.7
5.0	20.4	41.8	41.0
6.0	24.6	49.0	49.2
7.0	28.7	57.0	57.3
8.0	32.8	65.3	65.5
9.0	36.8	73.5	73.8
10.0	41.0	81.5	81.8
20.0	82.0	163.0	164.0

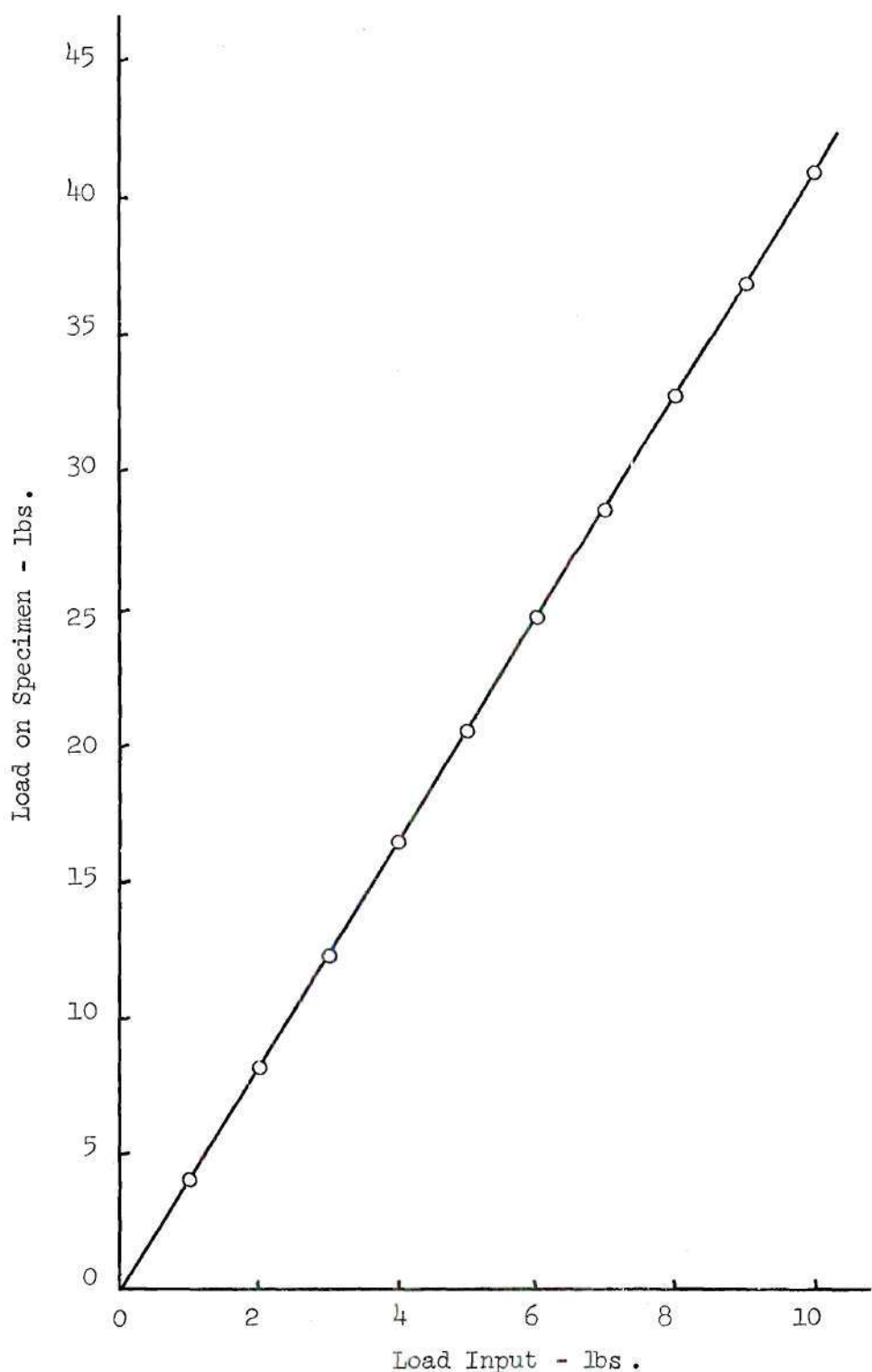


Figure 17. Calibration Curve for Position 1.

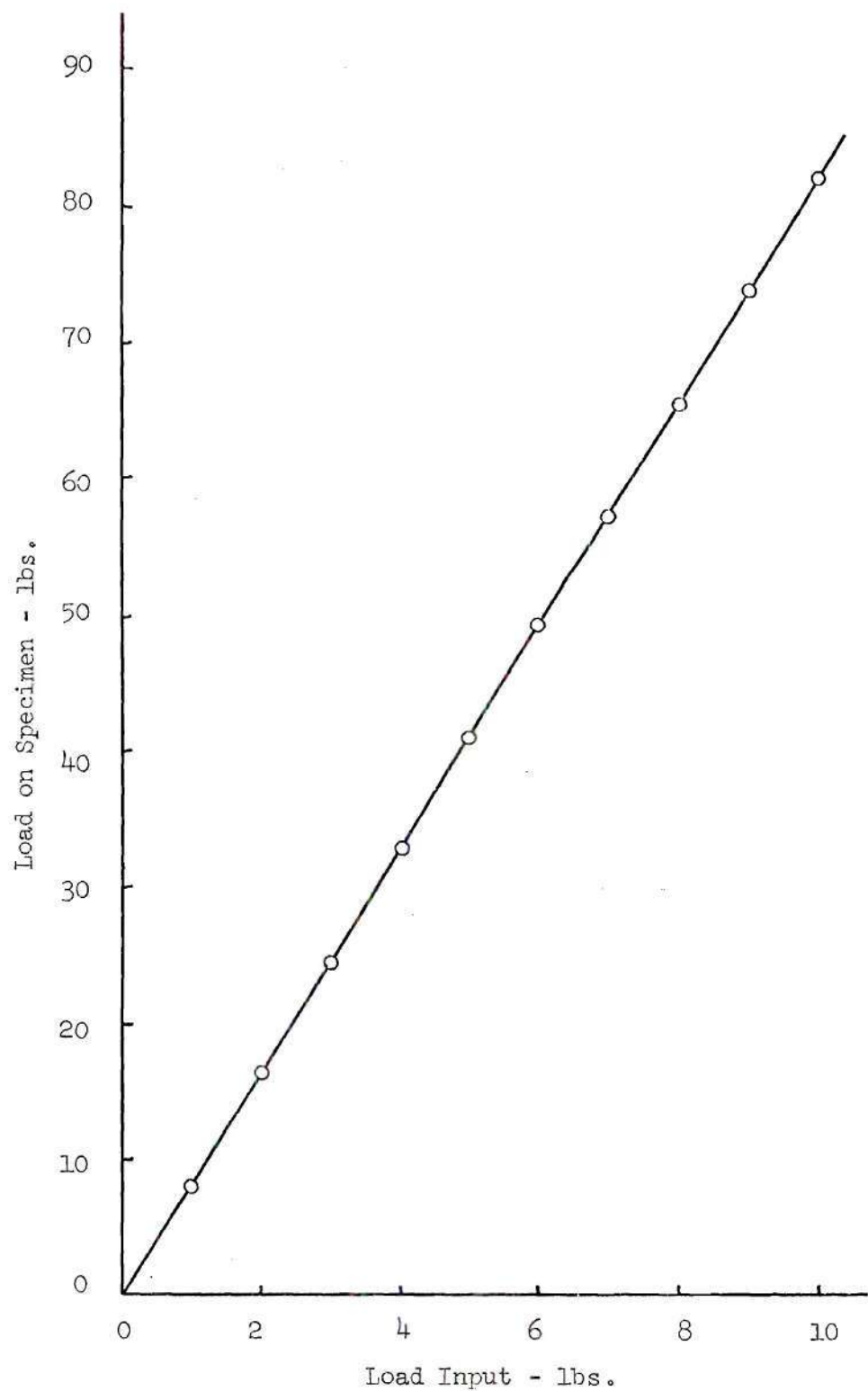


Figure 18. Calibration Curve for Position 2.

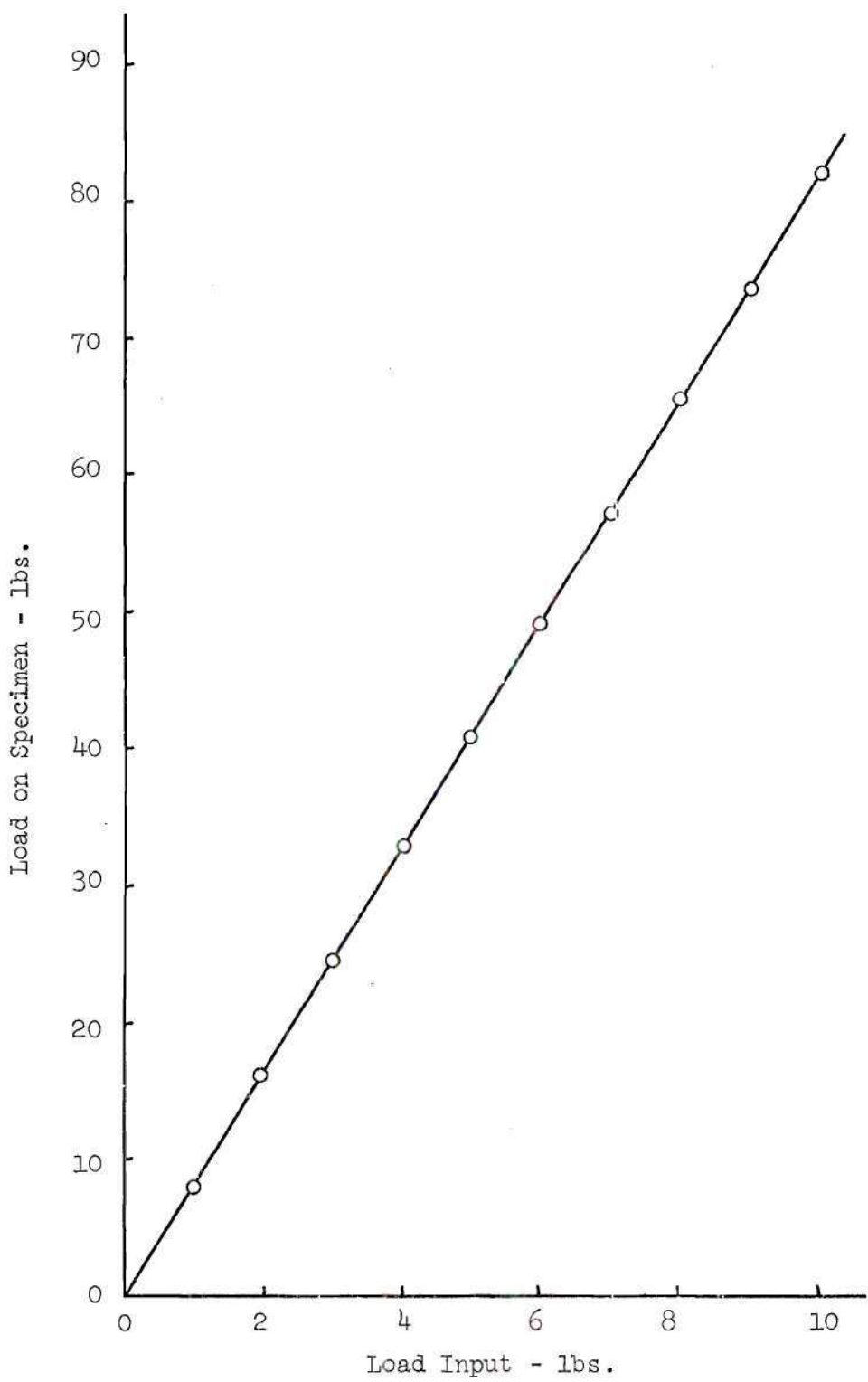


Figure 19. Calibration Curve for Position 3.

swaging, the surface impurities were again removed using 400 grit abrasive paper, polishing paper, and another dip in the macroetching solution.

Heat treating of the specimens for stress relief and crystal growth was necessary. This was done by first putting the specimens in glass capsules to minimize surface oxidation. Evacuation of the capsules and purging the capsules with argon proved useless in this respect, as the specimens tended to sublime under these conditions. The specimens were then placed in a temperature controlled furnace and held at  $750^{\circ}\text{F} \pm 25^{\circ}\text{F}$  for the required length of time. Stress relief of the specimens takes approximately two minutes. Crystal growth takes anywhere from two minutes up to 24 hours, depending upon the size of the crystal required. After removal from the furnace, the glass encapsulated specimens were air cooled, and after cooling the specimens were again macroetched, this time using 50 percent hydrochloric acid and distilled water. The specimens were then stored at room temperature.

#### Testing Procedure

After the transducer measuring system was calibrated testing could proceed. Test specimens were inserted into the specimen grips, which were held in a special jig. This was to avoid any possible bending of the specimen and to assure a consistent three inch gauge length. Position 1 was used in all tests. With the specimen in the grips and jig, the grips were placed in the apparatus. After removing the slack in the linkages, the jig was removed and the

specimen put into tension by applying the load. Loads used were Instron calibration weights. Details about the types of specimens and stresses used in each test can be found in the following sections concerning tests A, B, and C, and tensile testing. Graphs of specimen elongation versus time were produced from the transducer-amplifier-recorder system and used in the data analysis.

The length of each test is at least two hours in duration. It was established that the creep of zinc reaches the steady state condition after approximately one hour, as the value of the strain rate based on successive time increments after one hour produces a negligible change. In all cases, values of the steady state strain rate ( $\dot{\epsilon}_{ss}$ ) given in the results are based on the last 30 minutes of testing.

Measurement of the average grain size of each specimen that was tested is required. This is accomplished by the grain boundary intercept method, with measurements taken along the longitudinal axis of the specimen. That is, the number of grain boundaries intercepted by a line one inch long, taken at four randomly chosen places on the specimen are counted. The mean grain intercept or average grain size is then found by dividing the length of the line by the number of intersections counted, and averaging the four values.

All testing is done at  $20^{\circ}\text{C}$  (room temperature) which is  $0.42 T_m$  for zinc, and temperature is held constant in each test.

## CHAPTER III

## RESULTS

The results of this investigation include creep test data showing steady state strain rate dependence on grain size for the two specimen types tested, and a microscopic evaluation of specimens before and after testing. Also, data from tensile tests have been obtained in order to determine a yield point for the material used in the investigation, as well as the extent to which specimens could be strained.

Tensile Testing

The tensile properties of pure zinc in the polycrystalline and bamboo states were obtained using a standard Instron Tensile Tester. There were two reasons for determining these properties. First, it was necessary to determine a bound to the stress to be used in creep testing, such that it was sensibly near or below the yield stresses of the material. Second, it was of value to know what extensions could be expected from the specimens.

The results of the tensile tests are presented in Table 7. From the results of tensile testing it was established that the yield point for bamboo specimens, over the range of average grain sizes, remained relatively constant at approximately 300 psi. Extensions of up to 94 percent were observed in specimens with a large

Table 7. Tensile Test Results.

Test Number	Approximate Grain Size L - inches	$\sigma_{yield}$ psi	Temperature 20°C		Total Percent Elongation
			$\sigma_{ULT}$ psi	Gauge Length 3.0 in.	
1	0.160	220	2360	94.0	
2	0.160	180	2230	64.5	
3	0.160	235	1680	38.0	
4	0.080	325	1110	20.0	
5	0.080	235	1730	25.0	
6	0.040	325	2620	20.0	
7	0.040	325	4370	35.0	
8	polycrystal	12,600	16,400	30.0	
9	polycrystal	11,800	16,400	39.0	

average grain size, whereas this value drops significantly to 20 percent to 30 percent as the grain size decreases. The yield of polycrystalline specimens is reported at approximately 12,000 psi., with extensions of 30 percent to 40 percent attained.

From this data stresses of 236 psi. and 538 psi. were chosen for two creep tests on bamboo specimens. For a polycrystalline test, a stress of 818 psi. was chosen.

#### Creep Tests on Bamboo Specimens

The first creep test, Test A, was conducted on 15 bamboo structured specimens, with a diameter of .0695 inches, at a stress of 236 psi. A typical curve that was generated during the testing is given in Figure 20. Regions of transient and steady state creep are noted. The transition from transient to steady state creep occurred after approximately one hour. Tests were two hours in length and values of steady state strain rate were computed as described in the test procedure section. The results of Test A are given in Table 8 and are represented graphically in Figure 21.

There is a great deal of scatter in the data of Test A. The correlation coefficient produced by a least squares analysis of the data is 0.153. Consequently, drawing a curve through the data points is not meaningful.

Test B results are given in Table 9 and the graph of Figure 22. The scatter in the data remains, and a correlation coefficient of 0.11<sup>14</sup> was produced. It is noted that the strain rate of Test B increased by approximately a factor of 10 when compared with Test A.

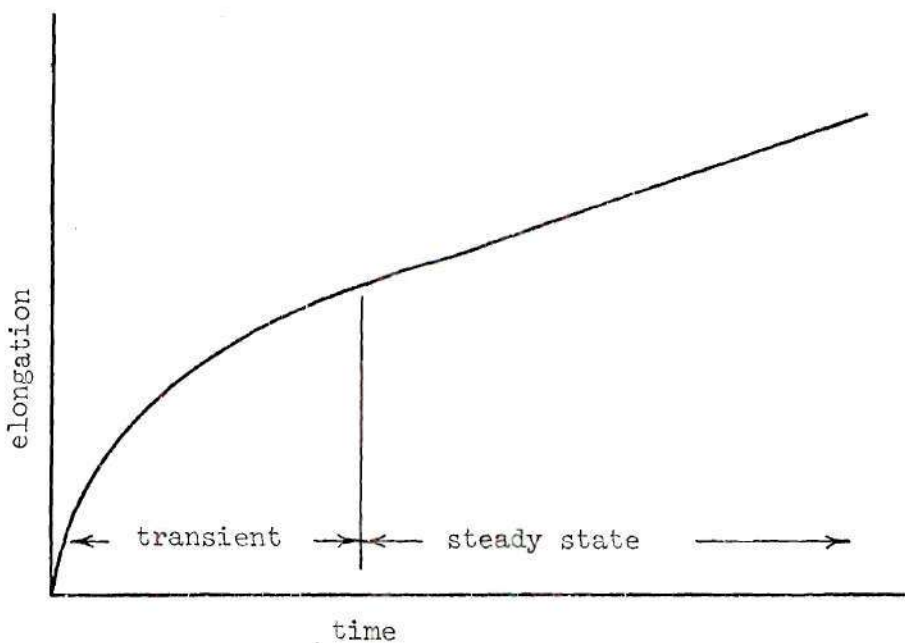


Figure 20. Typical Creep Curve for High Purity Zinc.

Table 8. Results of Creep - Test A.

Specimen Diameter 0.0695 in. Gauge Length 3.0 in. Load Input 100 gms.		Temperature 20°C Stress 236 psi
Test Number	$\dot{\epsilon}_{ss} \times 10^6 / \text{min}$	Average Grain Size L - inches
1	9.67	0.223
2	9.67	0.333
3	5.06	0.200
4	3.63	0.308
5	3.38	0.182
6	13.3	0.200
7	4.15	0.120
8	6.00	0.080
9	21.6	0.160
10	3.86	0.200
11	1.94	0.200
12	4.17	0.117
13	5.66	0.137
14	1.72	0.098
15	8.16	0.088

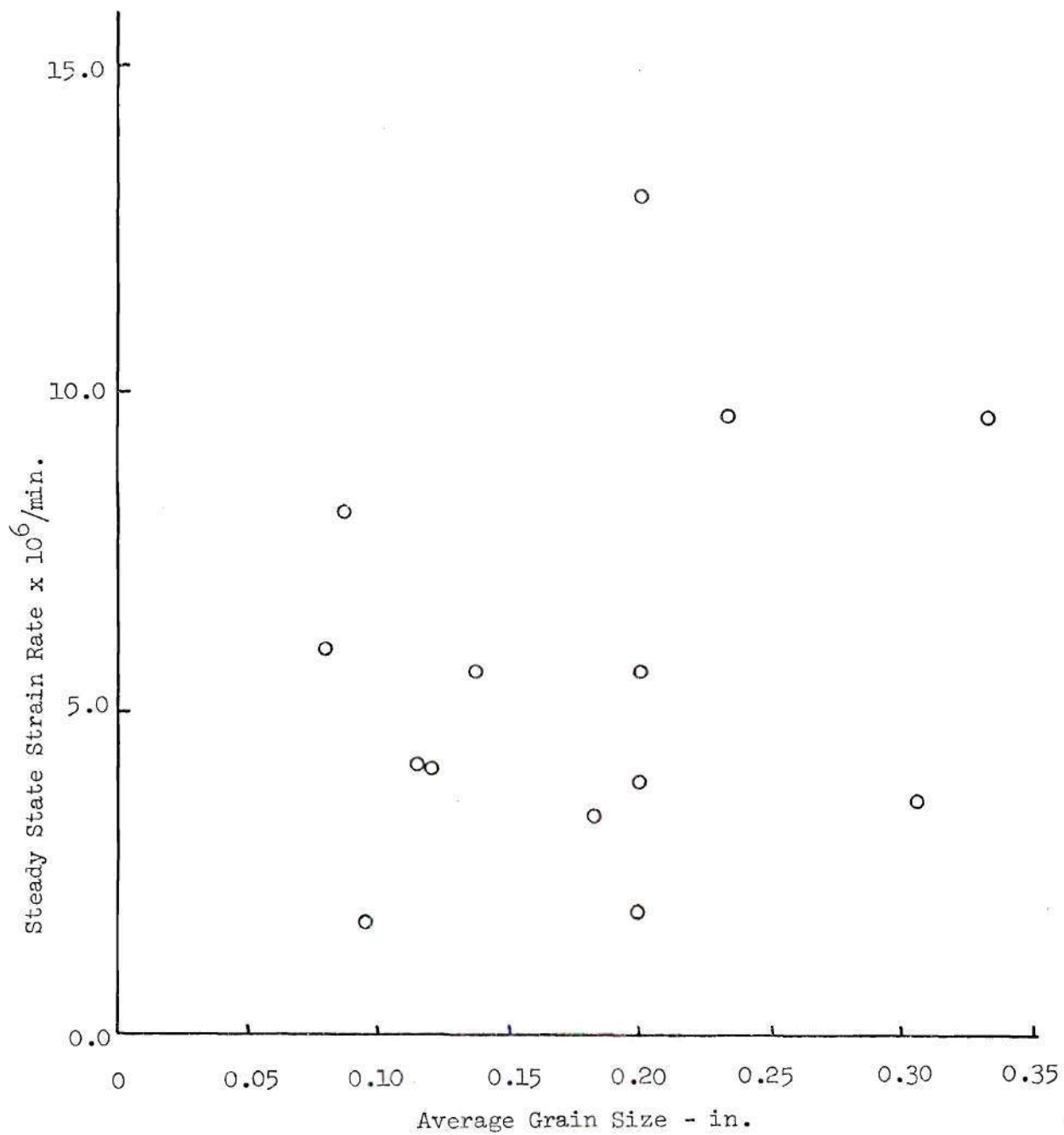


Figure 21. Steady State Strain Versus Average Grain Size for Test Set A.

Table 9. Results of Creep - Test B.

Test Number	$\dot{\epsilon}_s \times 10^5 / \text{min}$	Average Grain Size	
		Temperature 200°C	Stress 538 psi
1	3.34	0.103	
2	7.10	0.080	
3	4.83	0.089	
4	4.17	0.081	
5	6.50	0.096	
6	6.67	0.078	
7	8.86	0.096	
8	3.94	0.133	
9	5.27	0.089	
10	3.60	0.098	
11	3.60	0.100	
12	3.18	0.040	
13	4.17	0.222	
14	3.34	0.200	
15	3.34	0.175	
16	5.00	0.160	
17	3.90	0.147	
18	7.50	0.040	
19	6.13	0.133	
20	5.16	0.111	

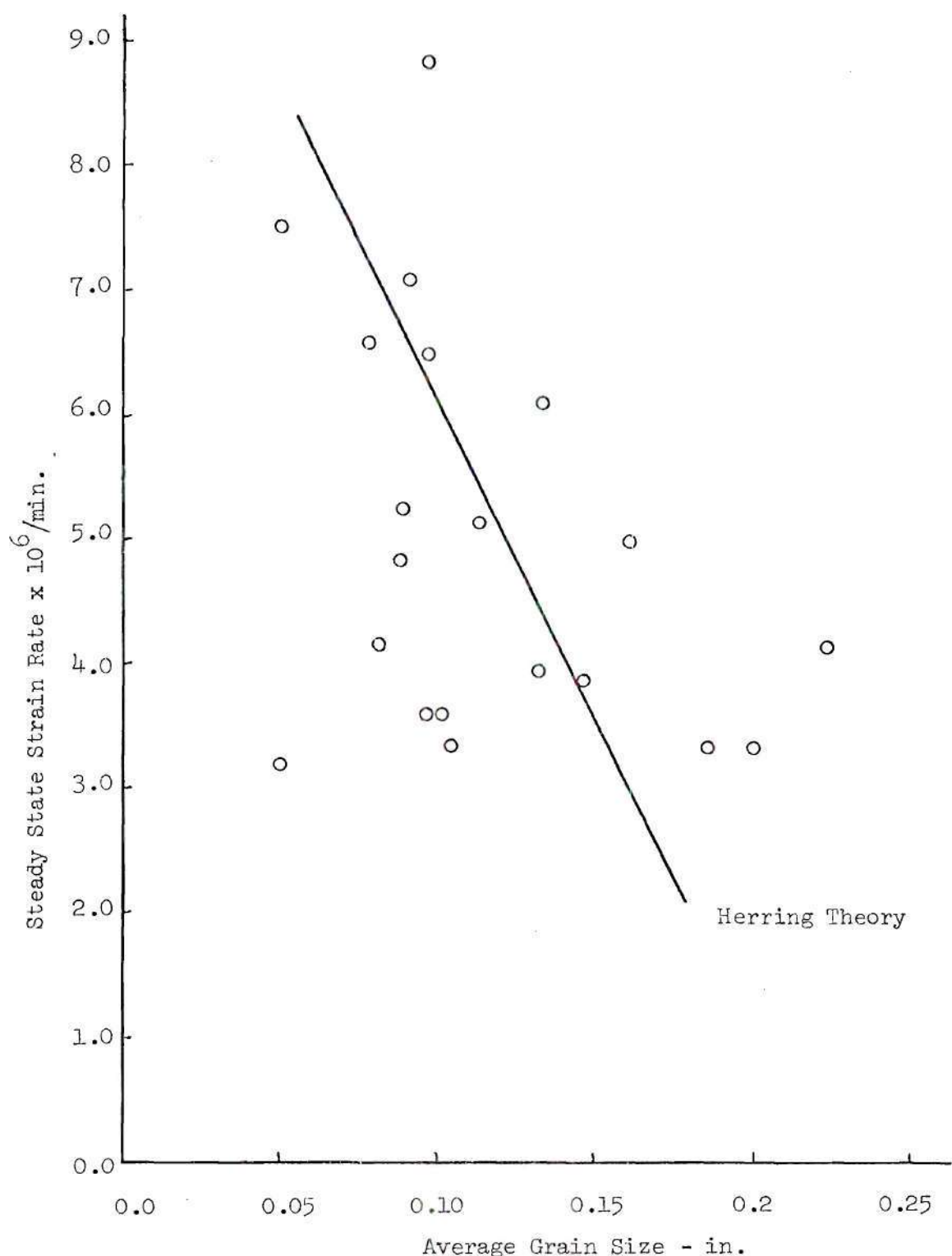


Figure 22. Steady State Strain Rate Versus Average Grain Size for Test Set B.

An increase in strain rate with increasing stress is expected, according to all creep theories.

According to the theory of Herring (refer to Table 1), the graphs of the data for Tests A and B should produce a straight line. This line is plotted for reference purposes on Figure 22. Once again, a linear regression analysis of the data of these tests shows a low correlation to a straight line.

#### Creep Tests on Coarse-Grain Polycrystalline Specimens

Test C was performed on coarse-grain polycrystalline specimens with a diameter of 0.25 inch, and at a stress of 818 psi. The results of creep tests on 12 specimens is given in Table 10, and are illustrated in the graph of Figure 23.

A linear regression of the data of Test C was performed using a least squares analysis. The results of the analysis are as follows:

Correlation Coefficient: 0.812/1.00

Intercept of the Line:  $2.37 \times 10^6$ /min.

Slope of the Line:  $-.645 \times 10^6$

The high correlation coefficient indicates that the straight line has a high correlation to test results.

The exponent of the grain size, according to this analysis is +1.0, and thus differs from all creep theory equations listed in Table 3. A graph of the theoretical results according to the Nabarro-Herring theory ( $\dot{\epsilon}_{ss} \propto 1/d^2$ ) is shown in Figure 23 for reference purposes, as it is the closest approximation to experimental results of those theories presented in Chapter I.

Table 10. Results of Creep - Test C.

Specimen Diameter .25 in.	Temperature 20°C	
Gauge Length 3.0 in.	Stress 818 psi	
Load Input 10.0 lbs.		
Test Number	Mean Grain Intercept mm.	$\dot{\epsilon}_{ss} \times 10^6 / \text{min}$
1	0.104	2.32
2	0.760	2.00
3	0.990	2.22
4	0.835	1.56
5	0.990	1.67
6	1.11	1.44
7	1.17	1.44
8	1.35	1.33
9	1.87	1.00
10	1.54	1.67
11	1.56	1.44
12	1.74	1.33

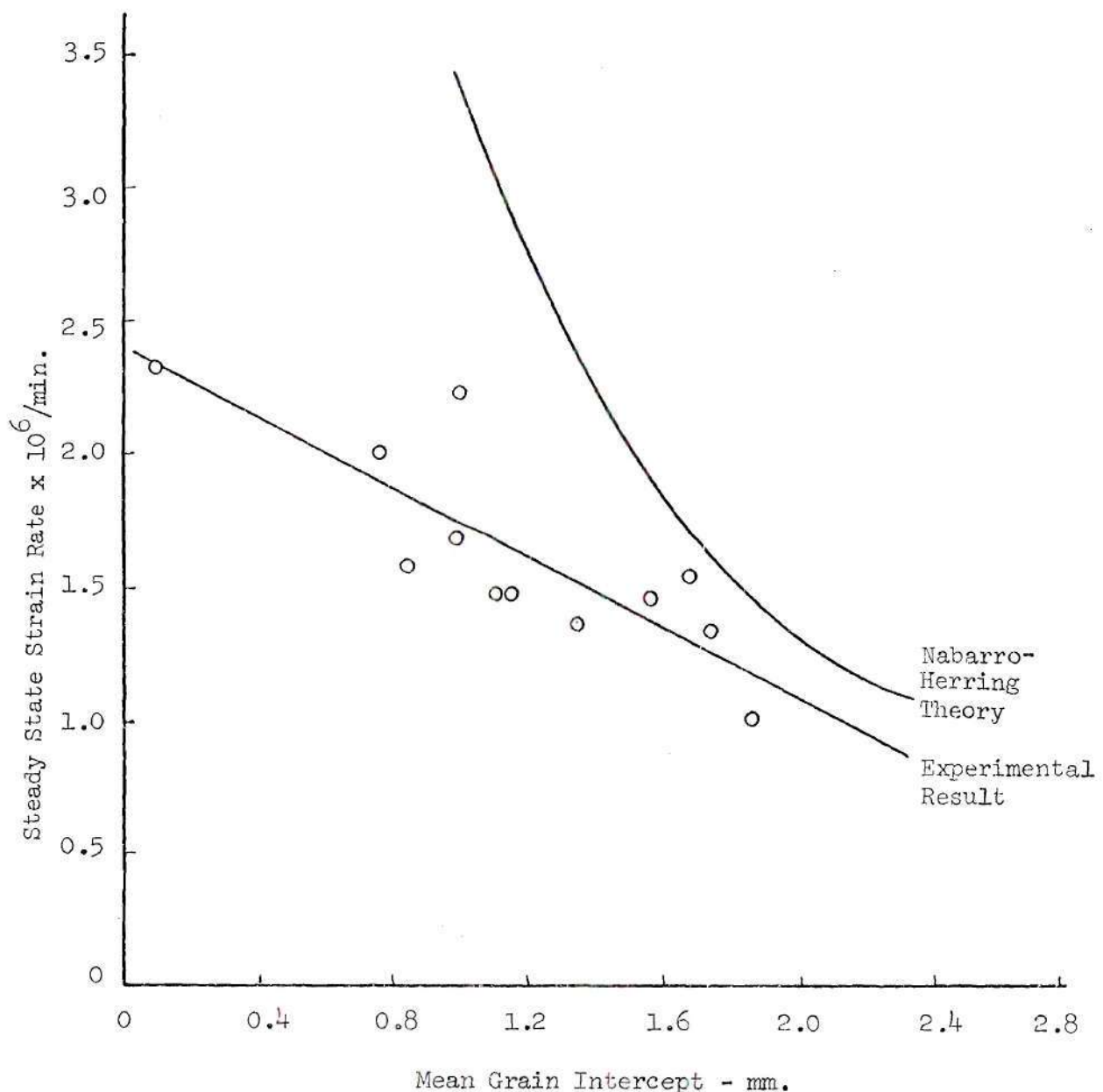


Figure 23. Steady State Strain Rate Versus Mean Grain Intercept for Test Set C.

Microscopic Investigation of Specimens

A microscopic study of specimens before and after testing was performed to determine if some observable change in specimen microstructure had taken place. The results are documented in the photographs of Figures 24 through 30.

Figure 24 is a photograph of the high purity zinc material as received and before any fabrication of specimens was done. It was received in the form of cast rods, and therefore the microstructure shows the typical columnar grain structure.

The photograph on Figure 25 shows the microstructure of a typical specimen after swaging. The picture is the cross section of a .25 inch diameter specimen. The microstructure of a 0.0695 inch diameter specimen shows a similar structure, but the grains are about half as large. The grains appear irregular and are in an unstable condition (i. e., has not been annealed to its more stable structure).

All specimens were annealed and heat treated as described in Chapter II to allow crystal growth and to relieve residual stresses. Figures 26 and 27 show microstructures of typical bamboo specimens and coarse-grain polycrystalline specimens, respectively. Figure 26 shows the segmentation that is required in a bamboo type specimen; crystals of approximately equal size, but different orientations, are stacked end to end. The photograph of Figure 27 shows the cross section of a 0.25 inch diameter specimen. The number of crystals in the cross section of such specimens varied between five and approximately 300. The grains have a structure that is stable and



Figure 24. Photograph of the Zinc Metal  
as Received. x10



Figure 25. Photograph of the Microstructure of Specimens After Swaging. x195

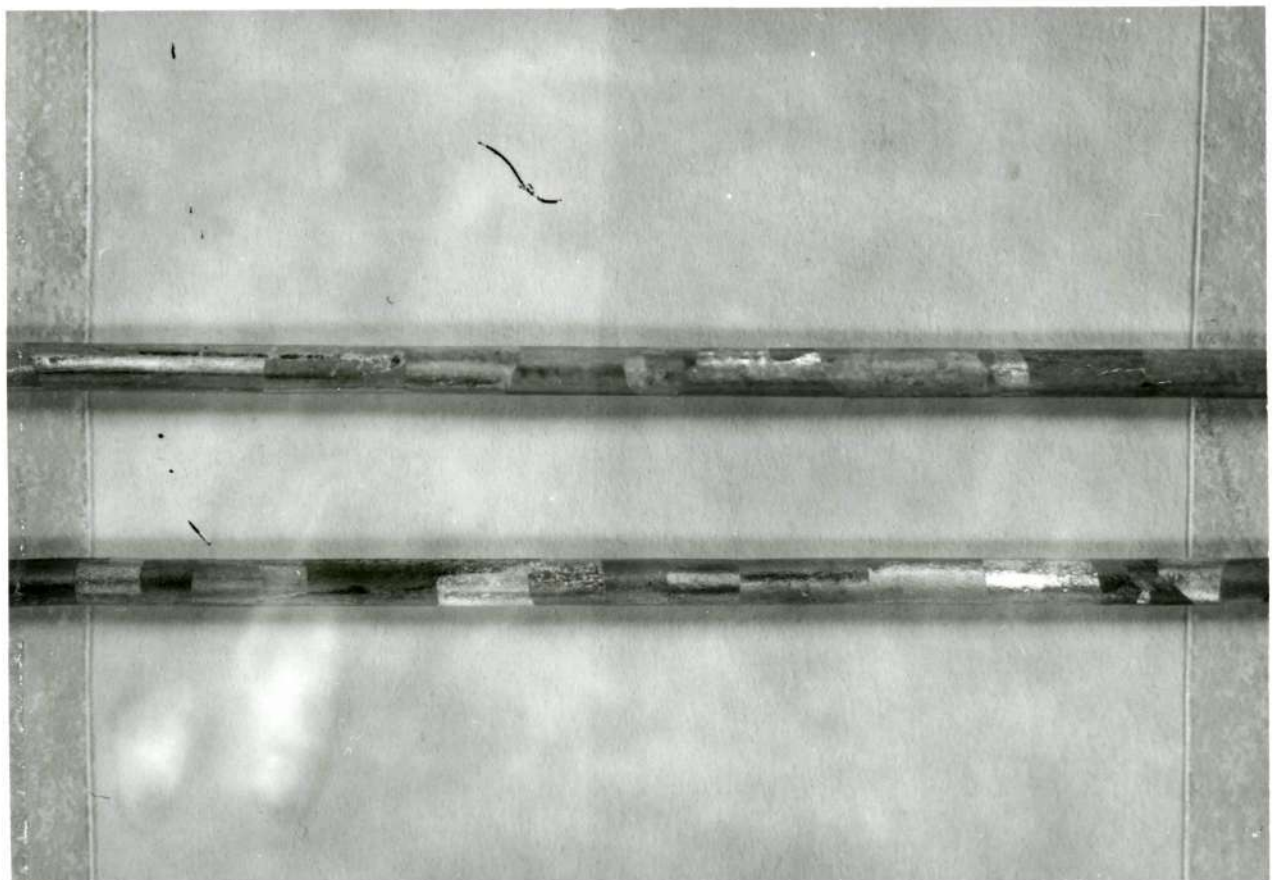


Figure 26. Photograph of Microstructure of Bamboo Specimens. x2



Figure 27. Photograph of the Microstructure of a Coarse-Grain Polycrystalline Specimen.  
x15

has been stress relieved.

The curious change in macroscopic appearance of bamboo specimens strained to fracture in tensile testing is shown in the photograph of Figure 28A. The specimen is seen to have areas where kinking and bending has occurred. In areas of highest strain, rotation of the slip plane has occurred to such an extent that the specimen has flattened out. Clam shell markings were observed on the surface of the specimen in these areas.

Figure 28B shows a bamboo specimen after a creep test. Of special interest in the photograph is an area that has necked sufficiently to cause a significant reduction in the cross sectional area. The necking was of the same nature as was observed in tensile test specimens after small elongations.

The photograph of Figure 29 was made to investigate this necked area further. The photograph is of the surface of a bamboo specimen taken at a higher magnification than Figure 28B. The axis of tension in the picture is vertical. Noted are the markings of twinning or slip of the crystal (the full area of the photograph is a single crystal). These are identical markings as was observed by Elam [20] and Miller [17] in their experiments with zinc single crystals. It is concluded that a large part of the total deformation of the crystals in a bamboo specimen is due to slip and twinning, as these markings were observable in all cases where necking was seen.

Microscopic examination of several cross sections of coarse-grain polycrystalline specimens showed similar marks as was observed

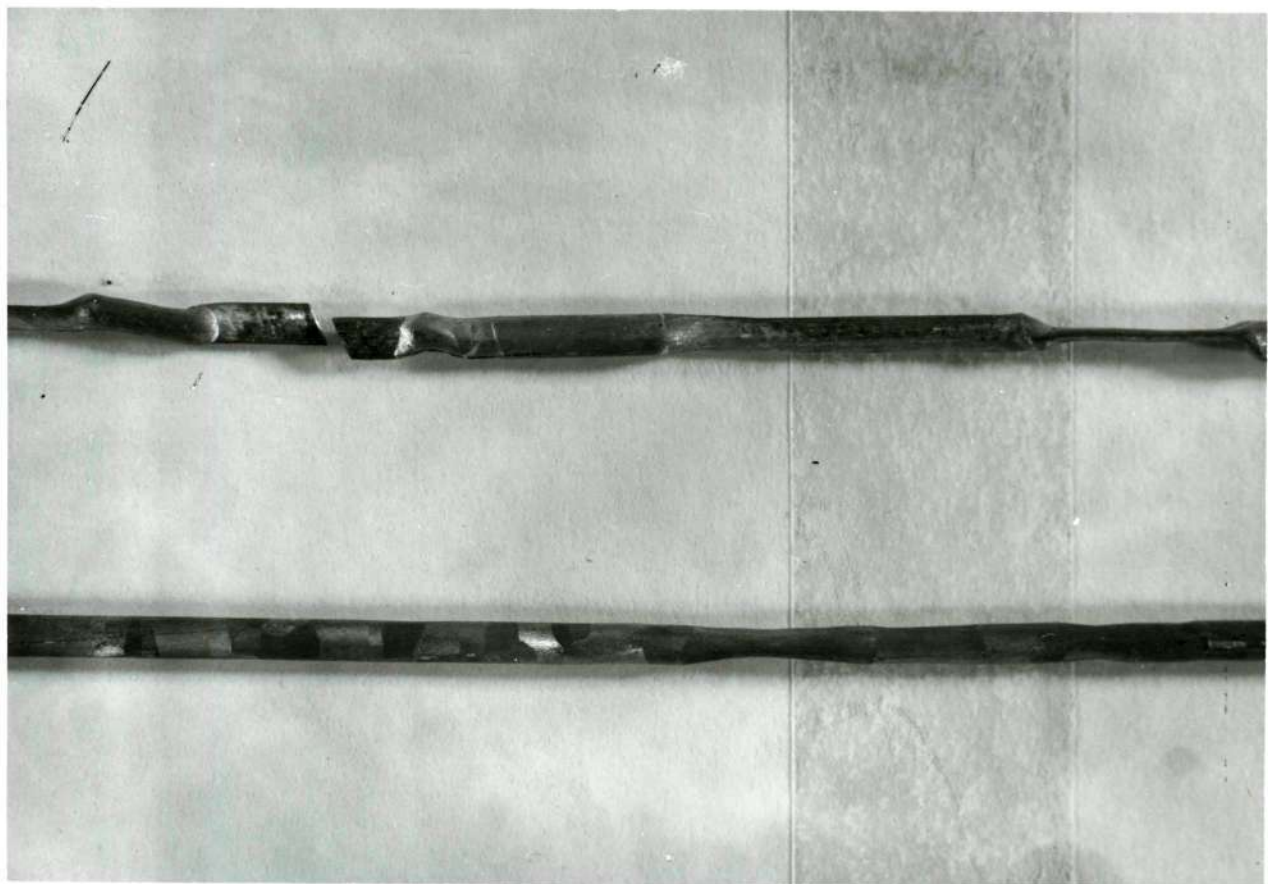


Figure 28A. Photograph of a Typical Specimen Strained to Fracture in a Tensile Test. x2

Figure 28B. Photograph of a Typical Specimen Strained in Creep Testing. x2



Figure 29. Photograph of the Necked Area of a Bamboo Specimen After a Creep Test. x95

in the bamboo structure. Typical of this are the marks shown in the photograph of Figure 30, which are slip and/or twinning marks. However, only select grains in the cross section of the specimen are seen to have these markings.



Figure 30. Photograph of the Cross Section of a Coarse-Grain Polycrystalline Specimen After Creep Testing. x95

## CHAPTER IV

## DISCUSSION

Bamboo Specimens

Referring to the results of creep tests on bamboo specimens (Tests A and B), the data show a great deal of scatter, and apparently the linear dependence of strain rate upon grain size as suggested by Herring, is inapplicable (refer to Figure 22). It should be noted that in the areas of the specimens where necking is observed, constant stress is not maintained and, in fact, are areas of locally higher stresses. The presence of slip or twinning marks in the necked areas indicates that the crystals in these areas are favorably oriented such that the critical resolved shear stress on the basal plane is reached, and therefore, the activation of the dislocation movements causing the deformation occurs in these areas first. The deformation of bamboo specimens may be viewed in terms of a "weakest link in a chain" analogy. The weakest links in the bamboo specimen are those crystals favorably oriented for slip and twinning to occur with relative ease compared with other crystals of different orientations. The deformation of the specimen is occurring mainly in these necked areas, and not uniformly throughout the specimen.

Coarse-Grain Polycrystalline Specimens

The data collected on the creep of zinc specimens in the

coarse-grain polycrystalline state requires a different analysis. No necking of the specimens is observed and the stress remains constant throughout the testing. Since all the crystals in the cross section of a specimen do not show the slip and twinning marks noted in the photograph of Figure 30, the unmarked crystals are those crystals in which the critical resolved shear stress is not reached. Therefore, while slip or twinning are definitely mechanisms of deformation, they are only two of the several that may be contributing to the total deformation of any crystal in the specimen.

Another possible deformation mechanism is vacancy diffusion. However, the diffusion theories of Nabarro, Coble, and Kosevich, et al. (refer to Table 3), do not predict the linear grain size dependence of strain rate that was established in Creep Test C. The mechanisms described by these theories, then, are not correctly describing the deformation of zinc in the coarse-grain polycrystalline state.

## CHAPTER V

## CONCLUSIONS

Based on the results of this investigation into the creep of high purity zinc, the following conclusions can be made:

- (1) Bamboo structured specimens deform mainly through slip and twinning of favorably oriented crystals.
- (2) Because of the effects of crystal orientation, bamboo specimens demonstrate an indeterminate relationship between grain size and steady state rate.
- (3) With respect to coarse-grain polycrystalline specimens, a linear relationship ( $n = 1.0$ ) between steady state strain rate and grain size is established, when stress and temperature are constant.
- (4) In coarse-grain polycrystalline specimens, deformation through slip or twinning occurs in only some of the crystals of the aggregate.
- (5) The data collected on the dependence of strain rate upon grain size for coarse-grain polycrystalline specimens does not agree with any of the common creep theories.

## CHAPTER VI

## RECOMMENDATIONS

Clearly, the grain size dependence of strain rate alone will not necessarily indicate which mechanisms are operating during deformation. All theories of creep indicate the stress and temperature dependencies of strain rate. Temperature dependence of strain rate could give the best indication of what mechanisms are operating by satisfactorily determining such quantities as activation energies for lattice and boundary self-diffusion. The stress dependence of strain rate also provides a means of determining deformation characteristics, since the grain size can be held constant and the stress varied in a creep test. In any case, a microscopic evaluation of test materials provides invaluable information concerning deformation.

If any future investigations into deformation mechanisms are undertaken, the best hope for deciding which creep mechanism is dominating the deformation under a particular set of circumstances, through mechanical testing, lies in examining each of the variables, namely a temperature, stress, grain size, and specimen microstructure.

## APPENDIX I

## CONSTANT STRESS DERIVATION

Consider the diagram of Figure 8 and define the following quantities:

$\ell_o$  = initial length of the specimen

$\ell$  = instantaneous length of the specimen

$\ell_H$  = length of the specimen when beam is horizontal

$A_o$  = initial area of the specimen

$A$  = instantaneous area of the specimen

$F$  = force on the specimen

$P$  = input load

$L_a$  = appropriate length on beam -  $L_1$ ,  $L_2$  or  $L_3$

$\theta$  = angular displacement of the beam from its horizontal position

The stress ( $\sigma$ ) on the test specimen is

$$\sigma = \frac{F}{A} \quad (1)$$

Also for small elongations

$$A\ell \approx A_o \ell_o \quad (2)$$

so

$$A = \frac{A_o \ell_o}{\ell} \quad (3)$$

Substituting (3) in (1) yields

$$\sigma = \frac{F}{A_o \ell_o / \ell} \quad (4)$$

From a balance of moments about the fulcrum

$$FL_1 \cos \theta = P(L_2 \cos \theta + L_3 \sin \theta) \quad (5)$$

Dividing by  $L_1 \cos \theta$  yields

$$F = P \left( \frac{L_2}{L_1} \frac{\cos \theta}{\cos \theta} + \frac{L_3}{L_1} \frac{\sin \theta}{\cos \theta} \right) \quad (6)$$

Simplifying

$$F = P \left( \frac{L_2}{L_1} + \frac{L_3}{L_1} \tan \theta \right) \quad (7)$$

It is known by geometry that

$$\tan \theta = \frac{\ell_H - \ell}{\sqrt{L_1^2 - (\ell_H - \ell)^2}} \quad (8)$$

Substituting (8) into (7) yields

$$F = P \left[ \frac{L_2}{L_1} + \frac{L_3}{L_1} \frac{(\ell_H - \ell)}{\sqrt{L_1^2 - (\ell_H - \ell)^2}} \right] \quad (9)$$

Substituting equation (9) into (4) yields

$$\sigma = \frac{P\ell}{A_o \ell_o} \left[ \frac{L_2}{L_1} + \frac{L_3}{L_1} \frac{(\ell_H - \ell)}{\sqrt{L_1^2 - (\ell_H - \ell)^2}} \right] \quad (10)$$

For stress to remain constant

$$\frac{d\sigma}{d\ell} = 0 \quad (11)$$

Differentiating equation (10) yields

$$\frac{d\sigma}{d\ell} = \frac{P}{A_o \ell_o} \left\{ \frac{L_2}{L_1} + \frac{L_3}{L_1} \left[ \frac{(\ell - 2\ell_H)(L_1^2 - (\ell_H - \ell)^2) + (\ell^2 - \ell\ell_H)(\ell_H - \ell)}{(\sqrt{L_1^2 - (\ell_H - \ell)^2})^3} \right] \right\} = 0 \quad (12)$$

But for small beam movements and specimen elongations

$$\ell \approx \ell_H \quad (13)$$

so

$$\ell - \ell_H \approx 0 \quad (14)$$

Simplifying (12) yields

$$0 = \frac{P}{A_o \ell_o} \left[ \frac{L_2}{L_1} + \frac{L_3}{L_1} \left( \frac{\ell}{L_1} \right) \right] \quad (15)$$

Finally, solving for  $\ell$  from (15) yields

$$\ell = \frac{L_2 L_1}{L_3} \quad (16)$$

which is the necessary design equation.

The differentiation of the complex term from equation (10) is as follows:

$$\text{Let } X = \frac{L_3}{L_1} (\ell_H \ell - \ell^2) (L_1^2 - (\ell_H - \ell)^2)^{-\frac{1}{2}}$$

$$\frac{dX}{d\ell} = \frac{d}{d\ell} \left[ \ell_o \ell (L_1^2 - (\ell_H - \ell)^2)^{-\frac{1}{2}} - \ell^2 (L_1^2 - (\ell_H - \ell)^2)^{-\frac{1}{2}} \right]$$

$$= \ell_H (L_1^2 - (\ell_H - \ell)^2)^{-\frac{1}{2}} - \frac{1}{2} (\ell_H) (L_1^2 - (\ell_H - \ell)^2)^{-3/2} (2\ell_o - 2\ell)$$

$$-2\ell (L_1^2 - (\ell_H - \ell)^2)^{-\frac{1}{2}} + \frac{1}{2} \ell^2 (L_1^2 - (\ell_H - \ell)^2)^{-3/2} (2\ell_H - 2\ell)$$

$$\frac{dx}{d\lambda} = \frac{\lambda - 2\lambda_H}{\sqrt{\lambda_1^2 - (\lambda_H - \lambda)^2}} + \frac{\lambda^2(\lambda_H - \lambda) - \lambda\lambda_H(\lambda_H - \lambda)}{(\sqrt{\lambda_1^2 - (\lambda_H - \lambda)^2})^{3/2}}$$

$$- \frac{\lambda - 2\lambda_H}{\sqrt{\lambda_1^2 - (\lambda_H - \lambda)^2}} + \frac{(\lambda^2 - \lambda\lambda_H)(\lambda_H - \lambda)}{(\sqrt{\lambda_1^2 - (\lambda_H - \lambda)^2})^3}$$

$$\frac{dx}{d\lambda} = \frac{(\lambda - 2\lambda_H)(\lambda_1^2 - (\lambda_H - \lambda)) + (\lambda^2 - \lambda\lambda_H)(\lambda_H - \lambda)}{(\sqrt{\lambda_1^2 - (\lambda_H - \lambda)^2})^3}$$

## APPENDIX II

## DERIVATION OF LOAD DECREASE FOR SMALL EXTENSIONS

Consider the specimen length shown below, undergoing creep with uniform elongation and define the following quantities:

$l_1$  = length of specimen at time  $T_1$

$P_1$  = load on specimen at time  $T_1$

$D_1$  = diameter of specimen at time  $T_1$

$A_1$  = cross section area of specimen at time  $T_1$

$l_2$  = length of specimen at time  $T_2$

$P_2$  = load on specimen at time  $T_2$

$D_2$  = diameter of specimen at time  $T_2$

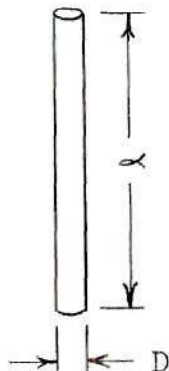
$A_2$  = cross section area of specimen at time  $T_2$

$V_1$  = volume of material in gauge length at time  $T_1$

$V_2$  = volume of material in gauge length at time  $T_2$

$\sigma_1$  = stress on specimen at time  $T_1$

$\sigma_2$  = stress on specimen at time  $T_2$



$$A_1 = \frac{\pi D_1^2}{4} \quad (1)$$

$$\sigma_1 = \frac{4P_1}{\pi D_1^2} \quad (2)$$

$$V_1 = \frac{\pi D_1^2 l_1}{4} \quad (3)$$

$$A_2 = \frac{\pi D_2^2}{4} \quad (4)$$

$$\sigma_2 = \frac{4P_2}{\pi D_2^2} \quad (5)$$

$$V_2 = \frac{\pi D_2^2 l_2}{4} \quad (6)$$

But for constant stress

$$\sigma_1 = \sigma_2 \quad (7)$$

Substituting (2) and (3) yields

$$\frac{4P_1}{\pi D_1^2} = \frac{4P_2}{\pi D_2^2} \quad (8)$$

Then

$$P_2 = \frac{P_1 D_2^2}{D_1^2} \quad (9)$$

For small elongations

$$v_1 = v_2 \quad (10)$$

Substituting (3) and (2) into (10) yields

$$\frac{\pi D_1^2 \ell_1}{4} = \frac{\pi D_2^2 \ell_2}{4} \quad (11)$$

Then

$$D_1^2 = \frac{D_2^2 \ell_2}{\ell_1} \quad (12)$$

Substituting (12) into (3) yields

$$P_2 = \frac{P_1 D_2^2 \ell_1}{D_2^2 \ell_2} \quad (13)$$

Finally

$$P_2 = \frac{P_1 \ell_1}{\ell_2} \quad (14)$$

## BIBLIOGRAPHY

1. Rosenhain, W., Haughton, J., Bingham, K., "Zinc Alloys with Aluminum and Copper," Journal of the Institute of Metals, Vol. 23, (1920), p. 261.
2. Pearson, C. E., "The Viscous Properties of Extruded Eutectic Alloys of Lead-Tin and Bismuth-Tin," Journal of the Institute of Metals, Vol. 54, (1934), p. 111.
3. Underwood, E. E., "A Review of Superplasticity," Journal of Metals, Vol. 14, (1962), p. 914.
4. Headley, T., Kalish, D., Underwood, E. E., "The Current Status of Applied Superplasticity," Burke, J., Weiss, V., Ultrafine-Grain Metals, Syracuse University Press, Syracuse, New York, (1970), pp. 325-353.
5. Holt, D. L., "Superplastic Fine-Grain Alloys in the Forming of Sheet Metal," Burke, J., Weiss, V., Ultrafine-Grain Metals, Syracuse University Press, Syracuse, New York, (1970), pp. 355-375.
6. Cornfield, G., Johnson, R., "The Forming of Superplastic Sheet Metal," International Journal of Mechanical Science, Vol. 12, (1970), pp. 479-490.
7. Dermott, R., "Extending the Possible in Metalworking," Metal Progress, Vol. 91, (1967), pp. 61-66.
8. Johnson, R., "Superplasticity," Metallurgical Reviews, Vol. 15, (1970), pp. 115-134.
9. Davies, G., Edington, J., Cutler, C., Padmanabhan, K., "Superplasticity: A Review," Journal of Materials Science, Vol. 5, (1970), pp. 1091-1102.
10. Weld, H., "Superplasticity," Report to the Department of Energy, Mines, and Resources, Canada, Information Circular 235, (1969), pp. 1-41.
11. Chaudhari, P., "Superplasticity," Science and Technology, Vol. 81, (1968), pp. 42-50.
12. Hayden, H., Floreen, S., Goodell, P., "The Deformation Mechanisms of Superplasticity," Metallurgical Transactions, Vol. 3, (1972), pp. 833-842.

13. Nicholson, R. B., "The Role of Metallographic Techniques in the Understanding and Use of Superplasticity," from Electron Microscopy and Structure of Materials, Edited by Thomas, G., Fulrath, R., Fisher, R., University of California Press, Berkeley, California, (1972), pp. 689-721.
14. Gilman, J. J., "Plastic Anisotropy of Zinc Monocrystals," Journal of Metals, Vol. 8, (1956), p. 1326.
15. Coffin, F., Weinan, A., "Surface Effects and Creep of Zinc Single Crystals," Journal of Applied Physics, Vol. 24, (1954), pp. 282-288.
16. Weinberg, E., "Creep of Zinc Single Crystals Under Direct Shear," Journal of Applied Physics, Vol. 24, 737, 1953.
17. Miller, "Creep and Twinning of Zinc Single Crystals," Transactions A.I.M.E., Vol. 122, (1936), p. 176.
18. Cotrell, A., Aytekin, V., "The Flow of Zinc Under Constant Stress," Journal of the Institute of Metals, Vol. 77, (1950), p. 385.
19. Tegart, M. E., Sherby, O., "Activation Energies for High Temperature Creep of Polycrystalline Zinc," Philosophical Magazine, Vol. 3, (1958), p. 1287.
20. Sully, A. H., Metallic Creep and Creep Resistant Alloys, Interscience Publishers, New York, (1949).
21. Herring, C., "Diffusional Viscosity in a Polycrystalline Solid," Journal of Applied Physics, Vol. 21, (1950), p. 437.
22. Nabarro, F. R. N., "Deformation of Crystals by the Motion of Single Ions," Report of a Conference on the Strength of Solids, Physical Society, London, (1948), pp. 75-90.
23. Udin, H., Shaler, A., Wulff, J., "The Surface Tension of Solid Copper," Journal of Metals, Vol. 1, (1949), p. 186.
24. Dushman, S., Dunnbar, L., Huthsteiner, H., "Creep of Metals," Journal of Applied Physics, Vol. 15 (1944), p. 108.
25. McLean, D., "Deformation at High Temperatures," Metallurgical Reviews, Vol. 7, (1962), pp. 481-527.
26. Weertman, J., "Steady State Creep of Crystals," Journal of Applied Physics, Vol. 28, (1957), pp. 1185-1189.

27. Nabarro, F. R. N., "Steady State Diffusional Creep," Philosophical Magazine, Vol. 16, (1967), p. 231-237.
28. Kosevich, A., Saralidze, Z., Slezov, V., "Diffusion-Dislocation Mechanism of Crystal Flow," translated, Soviet Physics JETP, Vol. 23, (1966), pp. 636-644.
29. Coble, R. L., "A Model for Boundary Diffusion Controlled Creep in Polycrystalline Materials," Journal of Applied Physics, Vol. 34, (1963), pp. 1679-1682.
30. McLean, D., Farmer, N., "The Relation During Creep Between Grain Boundary Sliding and Sub-crystal Size and Extension," Journal of the Institute of Metals, Vol. 85, (1957-1958), p. 41.
31. Sulley, A. H., "Present Advances in Knowledge Concerning Processes of Creep in Metals," Progress in Metal Physics, ed. Chalmers, B., King, R., Pergamon Press, New York, Vol. VI, (1958), p. 135.
32. Stevens, R. N., "Grain Boundary Sliding in Metals," Metallurgical Reviews, Vol. 11, (1966), pp. 129-142.
33. Stevens, R. N., "Calculation of Deformation Caused by Grain Boundary Sliding," Transactions of the Metallurgical Society of the A.I.M.E., Vol. 236, (1966), p. 1762.
34. Weertman, J., "Dislocation Climb Theory of Steady State Creep," A.S.M. Transactions, Vol. 61, (1968), pp. 681-694.
35. Weertman, J., "Theory of Steady State Creep Based on Dislocation Climb," Journal of Applied Physics, Vol. 26, (1955), p. 1213.
36. Weertman, J., "Steady State Creep Through Dislocation Climb," Journal of Applied Physics, Vol. 28, (1957), pp. 362-364.
37. Dorn, J., "The Spectrum of Activation Energies for Creep," Creep and Recovery, A.S.M. Publication, Cleveland, Ohio, (1957), pp. 255-283.
38. Dorn, J., "Progress in Understanding High Temperature Creep," A.S.T.M. Publication, Philadelphia, (1962), pp. 1-22.
39. Sherby, O., Orr, L., Dorn, J., "Creep Correlations of Metals at Elevated Temperatures," Journal of Metals, Vol. 6, (1954), p. 71.
40. Schoeck, G., "Theory of Creep," Creep and Recovery, A.S.M. Publication, Cleveland Ohio, (1957), pp. 199-226.
41. Jackman, L. A., "Low Temperature Transient Creep of Selected Body-Centered Cubic Metals and Binary Solid Solution Alloys," Ph.D. Thesis, Rensselaer Polytechnic Institute, Troy, New York, 1967, pp. 53-70.